

## **ABSTRACT**

Lewis, Mark Austin. End Milling of Elastomers. (Under the direction of Dr. Albert Shih)

The purpose of this study is to identify mechanisms for effective elastomer machining using sharp, woodworking tools and cryogenic cooling. The development of an elastomer machining process could reduce cost and time spent in mold processing as an alternative approach. Thirteen tools of different sizes, tool geometries, materials, and milling configuration are used in this study. Fixture design is identified to be critical to elastomer machining due to material's elastic properties. The finite element method using ANSYS software is used to evaluate the stiffness of the workpiece when machined by different size end mills. The term effective stiffness is defined for the elastomer workpiece and found to increase with increasing tool size. Down milling configuration tools can effectively remove elastomer material at room temperature. Cryogenic cooling to  $-78.6^{\circ}\text{C}$  with solid carbon dioxide also improves the machined elastomer surface. A survey of the chip morphology is taken using Scanning Electron Microscopy (SEM). A system of classifying 7 types of chips based on size and morphology is developed. Serrated chip formation with apparent adiabatic shear bands is observed for one end milling test, possibly caused by the low thermal conductivity of elastomers. Other serrated chips exhibit wavy marks on the surface possibly due to vibration during machining. Milling forces were recorded and analyzed and show higher cutting forces for samples cut at the cryogenic condition. Cutting forces also reveal a correlation of the maximum uncut chip thickness with averaged peak cutting forces for different spindle speeds, which may have potential for modeling the elastomer machining process.

# END MILLING OF ELASTOMERS

by

MARK AUSTIN LEWIS

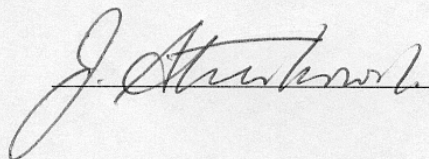
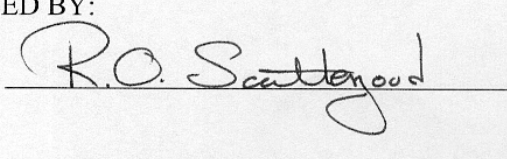
A thesis submitted to the Graduate Faculty of  
North Carolina State University  
in partial fulfillment of the  
requirements for the Degree of  
Master of Science

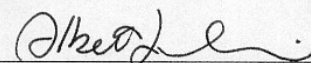
Department of Mechanical and Aerospace Engineering

Raleigh

2002

APPROVED BY:

 \_\_\_\_\_  \_\_\_\_\_

  
\_\_\_\_\_  
Chair of Advisory Committee

## **BIOGRAPHY**

Mark was born in Jacksonville, North Carolina. Growing up he had the privilege to live outside the continental U.S. and experience other cultures. During high school he enjoyed playing golf and being outdoors. He also excelled in math and science. This led him to attend engineering school at NC State where he was attracted to the hands-on aspect of Mechanical Engineering. After being introduced to manufacturing engineering on a summer internship, Mark began doing research and working towards a Master's Degree in Mechanical Engineering. From an eastern North Carolina town, Mark shall venture that direction upon graduation to Havelock, NC to work in the defense industry.

## **ACKNOWLEDGEMENTS**

The final product of this research has been a combined effort of many cooperating partners. Thanks to Dr. Albert Shih for his support, patience, and guidance throughout this project. Thanks to David Gill for giving his time and energy to run the equipment necessary to complete this project. Thanks to Jian Kong for taking several Scanning Electron Microscope pictures at Oak Ridge National Laboratory, and to Jun Qu for doing the same several times. Thanks to Adam Curry for his creation of the finite element model using ANSYS software used in this study. Thanks to Brian Rhoney for his assistance with LabVIEW software. Thanks to Darrin Poirier for his assistance in the analysis of experiment data. Thanks to Rick Lemaster, Supasit Rodkwan, and Dr. Greg Buckner for the use of special equipment. Thanks to Jie Luo for his help in conducting experiments, photography, and analysis.

Thanks to committee member Dr. Ron O. Scattergood for being on the committee. Thanks to John S. Strenkowski for his expertise in this research and for his part on the committee.

# TABLE OF CONTENTS

<b>LIST OF TABLES .....</b>	<b>vi</b>
<b>LIST OF FIGURES .....</b>	<b>vii</b>
<b>1 INTRODUCTION.....</b>	<b>1</b>
1.1 Mold Processing of Elastomers .....	1
1.1 References.....	5
<b>2 TOOL GEOMETRY AND TOOLS.....</b>	<b>6</b>
<b>3 PROPERTIES OF ELASTOMER MATERIALS.....</b>	<b>10</b>
3.1 References.....	12
<b>4 FIXTURE DESIGN .....</b>	<b>13</b>
4.1 Finite Element Analysis of Elastomer Workpiece Stiffness.....	15
4.2 References.....	21
<b>5 TEMPERATURE AND MILLING PARAMETERS.....</b>	<b>22</b>
5.1 Preliminary Elastomer Machining Tests.....	22
5.2 Overview of Experiments .....	23
5.3 Overview of Mechanisms that Influence Elastomer Machining.....	25
5.4 References.....	26
<b>6 EXPERIMENTATION .....</b>	<b>27</b>
6.1 Appearance of Machined Grooves.....	28
6.2 Effect of Tool Geometry .....	28
6.2.1 Tool Size.....	29
6.2.2 Up and Down Milling Configuration.....	30
6.2.3 Tool Material and Number of Flutes .....	30
6.3 Effect of Workpiece Temperature .....	32
6.4 Effect of Feed Rate and Spindle Speed.....	32
<b>7 CHIP MORPHOLOGY .....</b>	<b>36</b>
7.1 Chip Classification System.....	37
7.2 Discussion of Chip Types .....	42
7.2.1 Straight Flat Serrated Chip (SFE).....	42
7.2.2 Straight Curled Serrated Chip (SCE) .....	42

7.2.3 <i>Rough Flat Chip (RF)</i> .....	43
7.2.4 <i>Straight Curled Smooth and Rough Curled Chip (SCM and RC)</i> .....	43
7.2.4 <i>Burned Chip (B)</i> .....	43
7.2.5 <i>Straight Flat Smooth Chip (SFM)</i> .....	44
7.3 Correlation between Chip Characteristics and Groove Appearance.....	47
7.4 Effect of Spindle Speed and Feed Rate on Chip Morphology .....	48
7.5 References.....	50
<b>8 FORCES IN END MILLING ELASTOMERS</b> .....	<b>51</b>
8.1 References.....	57
<b>9 CONCLUSION</b> .....	<b>58</b>

## **LIST OF TABLES**

### **Chapter 1**

Table 1.1: Characteristics and Applications of 5 commercial elastomers [Harper, 1975 and Callister, 1997] .....	4
---	---

### **Chapter 3**

Table 3.1: Elastomer material properties compared to other common engineering materials [Gere and Timoshenko, 1997; Incropera and Dewitt, 1996]. .....	10
--	----

Table 3.2: Generic tire compound example for tread area of the tire [Bhowmick, 1994]. .....	11
---	----

### **Chapter 4**

Table 4.1: Results of finite element analysis for the effective stiffness of elastomer workpiece machined using three diameters of end mill. ....	20
---	----

### **Chapter 5**

Table 5.1: Summary of seven end milling experiments on flat elastomer samples.....	24
--	----

Table 5.2: Parameter matrix used for testing in Experiments IV – VII. ....	24
--	----

### **Chapter 6**

Table 6.1: Qualitative results for grooves machined in Experiments I – III. ....	29
--	----

Table 6.2: Qualitative results for grooves machined in Experiments IV – VII. ....	33
---	----

Table 6.3: Calculation of uncut chip thickness for parameters in Experiments IV – VII. ....	33
---	----

# LIST OF FIGURES

## Chapter 1

- Figure 1.1: A manually carved tire tread pattern [Michelin Americas R & D]. ..... 2
- Figure 1.2: Device invented by Clayton for milling of tire treads [Clayton, 1982]. ..... 3

## Chapter 2

- Figure 2.1: Various cutting configurations of wood working end mills manufactured by Onsrud Cutter LP; (a) down milling, (b) up milling, and (c) mixed milling end mills; (d) down milling setup, (e) up milling setup, and (f) mixed milling setup. .... 7
- Figure 2.2: Thirteen end mills manufactured by Onsrud Cutter LP selected to study elastomer machining (HSS: high speed steel)..... 8

## Chapter 4

- Figure 4.1: Fixture for end milling of elastomer A) base and top plate with slots and B) overhead view with elastomer workpiece..... 14
- Figure 4.2: Cross section A from Figure 4.1 of fixture for elastomer machining showing end milling slots and workpiece deformation. .... 14
- Figure 4.3: Description of three dimensional finite element meshes and boundary conditions for the elastomer workpieces machined by (a) 3.18 mm diameter end mill, (b) 6.35 mm diameter end mill, and (c) 12.70 mm diameter end mill. .... 16
- Figure 4.4: Traction stress (a) uniformly distributed on the quarter cylindrical surface in the Z direction, (b) at the eight nodes of a hexahedral element with the element resultant force,  $F_e$ , and (c) distributed as force vectors on the elements of the quarter cylindrical surface. .... 19

## Chapter 5

- Figure 5.1: Results of preliminary elastomer end milling tests that failed to make a clear cut groove on a workpiece with steel cable reinforcement (a) front view and (b) overhead view. .... 23
- Figure 5.2: Description of maximum uncut chip thickness for a two flute tool. .... 26



## Chapter 6

Figure 6.1: Examples of qualitative ratings for machined elastomer grooves.....	28
Figure 6.2: Grooves machined by the 13 tools in Experiments I and III.....	31
Figure 6.3: Grooves machined in Experiments V and VII, () indicates groove appearance rating.....	34

## Chapter 7

Figure 7.1: Optical pictures of elastomer chip collected from Experiments I and III, () represents groove appearance rating.....	38
Figure 7.2. The four-step procedure used to categorize chip morphology for an end milled elastomer.....	41
Figure 7.3: SEM micrographs of adiabatic shear band in the SFE type chip machined by Tool 8 in Experiment VII, 14.8 mm/s feed rate and 4200 rpm spindle speed, (a) overview of the chip and (b) close-up view shear band in the box in (a).....	44
Figure 7.4: SEM micrographs of (a) a curled, serrated SCE type chip with wavy marks machined by Tool 8 in Experiment III, (b) a SFE type of chip with the wavy serration mark on the surface.....	45
Figure 7.5: SEM micrographs of a RF type of chip machined by Tool 8 in Experiment I.....	45
Figure 7.6: SEM micrographs of SCM type curled chip machined by Tool 11 in (a) Experiment I and (b) Experiment III.....	46
Figure 7.8: SFM chip machined by Tool 4 at 5500 rpm and 14.8 mm/s feed rate.....	47
Figure 7.9: Optical pictures of chip formation in the four corners of the test matrix in Experiment V, Tool 6 at (a) 2900 rpm, 2.12 mm/s feed, (b) 2900 rpm, 14.8 mm/s feed, (c) 5500 rpm, 2.12 mm/s feed, and (d) 5500 rpm, 14.8 mm/s feed. ( ): Appearance rating of end milled groove.....	49

## Chapter 8

Figure 8.1: Definition of the directions of force components and general direction of the three force components generated by down milling Tool 6 on the elastomer workpiece.....	51
---	----

Figure 8.2: Three end milling force components vs. time for Tool 6 in Experiments I and III (4200 rpm and 12.7 mm/s feed rate)..... 52

Figure 8.3: Three end milling force components vs. time at the four corners of the test matrix in Experiment V: Tool 6, carbon dioxide cooled workpiece. [ ]: maximum uncut chip thickness in  $\mu\text{m}$ . ..... 54

Figure 8.4: Average peak milling forces vs. maximum uncut chip thickness in Experiment V at 2900 and 4200 rpm..... 56

# **1 INTRODUCTION**

Elastomers are used in a wide variety of everyday materials comprising tires, footwear and treads of shoes, grips, seals, and vibration and insulation components. The primary process to manufacture these products is the use of rubber molds. Rubber molds, especially footwear and tread making molds can be expensive and time consuming to produce. New innovative techniques to process elastomers should be explored to provide cost effective alternatives to rubber molds. This study focuses on the technique of machining elastomers. Specifically, the goal of this study is to explore the fundamentals of the process of elastomer machining and help identify mechanisms that provide favorable elastomer machining results.

Primarily, the use of cryogenic cooling and sharp woodworking tools is used to distinguish advantages and disadvantages in machining conditions. A clear-cut groove with full material removal is beneficial in elastomer machining.

## **1.1 Mold Processing of Elastomers**

Many common components consist of elastomers, such as gaskets, hoses, wear and grip pads, and vibratory and electrical insulation. To make these and other elastomer products, raw materials are combined with additives and heated, melted and injected or poured into a mold. The mold then undergoes a temperature, pressure, time cycle, which cures the elastomer to give it useful properties. The part geometry reflects the shape of the mold.

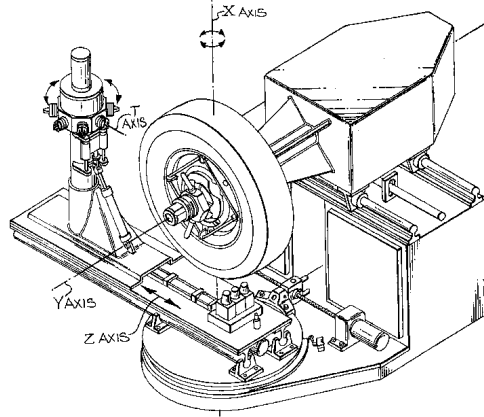
One of the largest elastomer industries is the tire industry. To manufacture a set of tire molds can cost between \$50,000 - \$80,000 and take up to 3 weeks [Gallego, 1998].

Other manufacturing processes to manufacture molds are under development, such as 5-axis CNC milling, 3D layer printing and sintering and fast graphite electrode machining for die sinking EDM. A process using a CNC machine to mill tire tread patterns could provide a considerable cost savings to tire industry in low batch production and prototype tire manufacturing. Currently, tire companies such as Michelin generate prototype tires to facilitate uses of specialty tires in car shows and auto racing. For these applications a worker manually carves a stenciled pattern into a slick tire with an electrically heated hand tool. A sample of a tire carved by hand using a similar hand tool is displayed in Figure 1.1.

The hand tools have interchangeable sharp blades of varying widths to produce the dissimilar widths seen in the tire's features. The carving operation is laborious and time consuming. Elastomer machining could lead to a process utilizing a CNC machine to mill the grooves. A machining process could reduce cost and throughput times in the prototype and performance tire generation in specialty markets. Clayton [1982] has patented equipment for application of tire tread milling. A picture of Clayton's apparatus is shown in Figure 1.2. However, due to lack of a feasible process the idea has not been developed.



*Figure 1.1: A manually carved tire tread pattern [Michelin Americas R & D].*



*Figure 1.2: Device invented by Clayton for milling of tire treads [Clayton, 1982].*

Other elastomer product industries share a similar production burden as the tire industry in making molds. Shoes are also produced using molds and may gain a savings in manufacturing costs and an added degree of customization with a rubber machining process. Customized footwear products are not popular because of the long lead time and high cost in manufacturing molds. Other elastomer products such as vibration isolators, dampers, golf grips, couplings, and press sensitive products like seals and gaskets could be more customized with the use of an elastomer machining process. Table 1.1 provides examples of some natural and man-made elastomers such as Natural Rubber and Styrene, their elongation to fracture, major characteristics and the products associated with them.

*Table 1.1: Characteristics and Applications of 5 commercial elastomers [Harper, 1975 and Callister, 1997]*

<b>Chemical type</b>	<b>Trade name</b>	<b>Elongation to fracture (%)</b>	<b>Major Characteristics</b>	<b>Typical Applications</b>
Natural polyisoprene	Natural rubber (NR)	500—760	Excellent physical properties; good resistance to cutting, gouging, and abrasion; low heat, ozone, and oil resistance; good electrical insulator	Pneumatic tires and tubes; heels and soles; gaskets
Styrene – butadiene copolymer	GRS, Buna S (SBR)	450—500	Good physical properties; excellent abrasion resistance; not oil, ozone, or weather resistant	Same as natural rubber
Acrylonitrile – butadiene copolymer	Buna A, Nitrile (NBR)	400—600	Excellent resistance to vegetable, animal, and petroleum oils; poor low-temperature properties	Gasoline, chemical, and oil hose; seals and O-rings, heels and soles
Chloroprene	Neoprene (CR)	100—800	Excellent ozone, heat, oil, and weathering, flame resistance	Wire, cable, belts, hoses, seals, chemical tank linings, and gaskets
Polysiloxane	Silicone (VMQ)	100—800	Excellent resistance to high and low temperatures; low strength, excellent electrical insulator	High- and low-temperature insulation; seals; diaphragms; tubing for food and medical uses

To evaluate the machinability of elastomers, this study focused on the end milling of elastomers. The appearance of end milled grooves were investigated and classified into four appearance ratings, and the effect of cryogenic cooling on elastomers was assessed. The cutting forces were measured to evaluate machining results and identify mechanisms of effective elastomer machining. Thirteen different end mills were used in a series of seven experiments and 87 milling tests to examine elastomer machining.

## 1.1 References

Callister, C., 1997, *Materials Science and Engineering*, 4<sup>th</sup> Ed., Wiley.

Clayton, A. R., 1982, *Tire Tread Grooving Apparatus and Method*, US Patent No. 4,311,182.

Gallego, Juan-Pablo, 1998, private communication.

Haper, C. (Ed.), 1975, *Handbook of Plastics and Elastomers*, McGraw-Hill.

## **2 TOOL GEOMETRY AND TOOLS**

Modern metal working machines are equipped to automatically change tools and cutting parameters dictated by the computer numeric control (CNC) system. A modern machining center has the ability to consistently generate precise cutting movements and is an excellent device to study elastomer machining. The CNC 3-axis Haas VF-1 vertical machining center at the Mechanical and Aerospace Engineering Department at N.C. State University was used in this study.

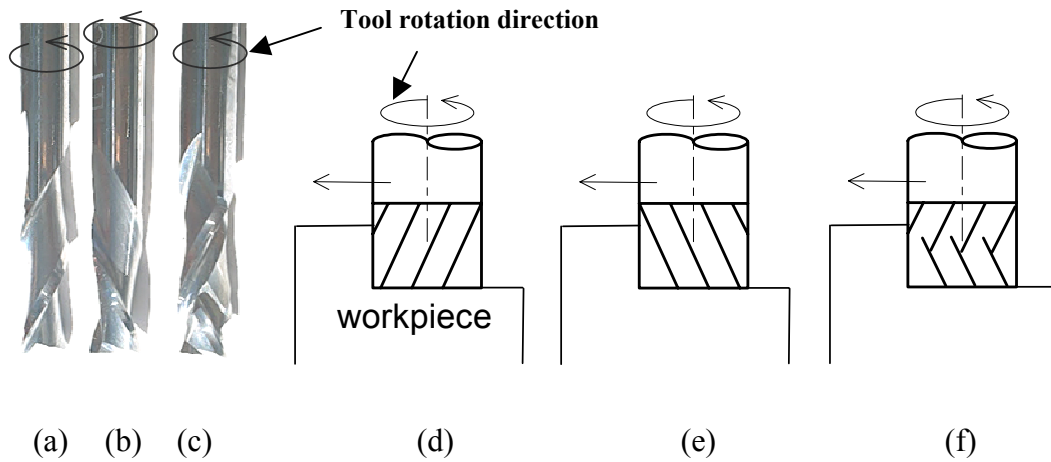
Standard end milling tools are made of high-speed steel and carbide with two to four flutes. Metal working end mills vary in size measured by cutting edge diameter, length, and geometry such as helix angle, and tip geometry. Helix angles vary from 20° - 40° for typical high-speed steel end mills and generally include standard tip geometry or a ball nose tip.

In contrast, end milling tools used in the woodworking industry have slightly different tip geometry, and dissimilar cutting configurations. Woodworking tools are chosen for this study to explore their unique geometric features on the effectiveness of machining elastomers. Additionally, woodworking tools are sharper than standard metal working tools.

Standard metal machining tools use an up milling cutting configuration, where chip debris is pulled to the surface of the workpiece from the tool tip as it breaks away from the material. Woodworking tools include a down milling configuration in which the flutes wind around the tool in the opposite direction to push chip debris from the surface of the workpiece toward the tool tip. The down milling configuration, illustrated in

























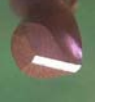
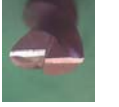


Figure 2.1, provides a smoother surface finish in wood and plastics and is used to study the effectiveness of elastomer machining.



*Figure 2.1: Various cutting configurations of wood working end mills manufactured by Onsrud Cutter LP; (a) down milling, (b) up milling, and (c) mixed milling end mills; (d) down milling setup, (e) up milling setup, and (f) mixed milling setup.*

Specifically, thirteen woodworking end mills manufactured by Onsrud Cutter LP were chosen to study the fundamentals of elastomer machining. The thirteen tools consisted of different tip geometries, helix angles, diameters, number of flutes, tool materials, and milling configuration. The thirteen tools are shown with their characteristics in Figure 2.2.

Tool #:	1	2	3	4	5	6	7
							
							
Diameter (mm):	3.18	3.18	3.18	6.35	6.35	6.35	6.35
Material:	Carbide	HSS	HSS	HSS	Carbide	Carbide	HSS
Helix:	Down	Down	Down	Down	Down	Down	Down
# of Flutes:	2	1	2	1	1	2	2
Helix angle (deg):	30	21	21	25	21	30	25
Onsrud Tool #:	57-240	40-002	40-102	40-006	62-775	57-280	40-108
Tool #:	8	9	10	11	12	13	
							
							
Diameter (mm):	6.35	6.35	6.35	6.35	12.7	12.7	
Material:	Carbide	HSS	Carbide	HSS	HSS	HSS	
Helix:	Up	Up	Up	Up	Down	Down	
# of Flutes:	2	1	1	2	1	2	
Helix angle (deg):	30	25	21	25	20	32	
Onsrud Tool #:	52-280	40-005	63-775	40-107	40-044	40-144	

*Figure 2.2: Thirteen end mills manufactured by Onsrud Cutter LP selected to study elastomer machining (HSS: high speed steel).*

Little information was available on tool selection for machining elastomer so a general batch of tools was selected to test effects of tool size, material, and geometry on elastomer machining. In general four original pairs of 6.35 mm tools were chosen on the basis of four different basic tip geometries. Tools 7 and 11 have a standard tip geometry with two flutes and tools 4 and 9 have a standard tip with one flute. The standard tip

tools were made of high-speed steel and had a helix angle of 25°. The O-flute tip geometry consists of tools 5 and 10, while tools 6 and 8 contain the wood rout tip. The non-standard tip geometries were made of carbide and had helix angles of 30° for the wood rout, and 21° for the O-flute. One of the tools in each of the four pairs was a down milling tool.

Five additional down milling tools were added to the four original pairs. Three 3.18 mm diameter tools and two 12.7 mm diameter tools were included to examine the effect of tool size on effective elastomer machining.

The thirteen tools can be summarized into three different tool series. Tools in a series have the same basic tip geometry, but can vary according to milling configuration, helix angle, and number of flutes. The three tool series according to Figure 2.2 are as follows:

- Standard Series:           Tools 2, and 3 (3.18 mm diameter, 21° helix angle)
- Tools 4, 7, 9, and 11 (6.35 mm diameter, 25° helix angle)
- Tool 12 (12.7 mm diameter, 20° helix angle)
- Tool 13 (12.7 mm diameter, 32° helix angle)
- Wood Rout Series:        Tool 1 (3.18 mm diameter, 30° helix angle)
- Tools 6 and 8 (6.35 mm diameter, 30° helix angle)
- O-flute Series:           Tools 5 and 10 (6.35 mm diameter, 21° helix angle)

Tools from the three series were tested for the effectiveness of milling a clear groove in an elastomer surface.

### 3 PROPERTIES OF ELASTOMER MATERIALS

Elastomers can be described as high molecular weight polymers that may experience large and reversible elastic deformation [Callister, 1997]. The stretchy, flexible characteristics make elastomers a good choice for vibration, insulation, absorption, and sealing. Natural rubber and many synthetic elastomers are used to develop tire compounds and other elastomer products. Table 3.1 describes elastomer properties compared to other materials.

*Table 3.1: Elastomer material properties compared to other common engineering materials [Gere and Timoshenko, 1997; Incropera and Dewitt, 1996].*

Material	Elastic modulus (GPa)	Poisson ratio	Ultimate stress (MPa)	Percent of elongation to fracture	Thermal conductivity (W/m · K)
Elastomers	0.0007 – 0.004	0.47 – 0.5	7 – 20	100 – 800	0.13 – 0.16
Aluminum alloy	70 – 79	0.33	100 – 550	1 – 45	177 – 237
Cast iron	83 – 170	0.2 – 0.3	69 – 480 (tension) 340 – 1400 (comp.)	0 – 1	70 – 80
Steel, high-strength	190 – 210	0.27 – 0.3	550 – 1200	5 – 25	35 – 60
Steel, spring	190 – 210	0.27 – 0.3	700 – 1900	3 – 15	40 – 50
Steel, stainless	190 – 210	0.27 – 0.3	400 – 1000	5 – 40	13 – 15
Plastic, Nylon	2.1 – 3.4	0.4	40 – 80	20 – 100	0.3
Plastic, Polyethylene	0.7 – 1.4	0.4	7 – 28	15 – 300	0.4

Elastomers' low modulus of elasticity contributes to their high percentage elongation before fracture. They also demonstrate significant hysteresis phenomena contributing to their energy absorption ability. Double bonds between Carbon atoms in elastomers permit curing and crosslinking and contribute to elastomers' viscoelastic characteristics.

The viscoelastic response of elastomer compounds forms the fundamental relationship between the compound and its properties [Bhowmick, 1994]. Stiffness, dynamic modulus, flexural strength, and tear resistance are some typical properties of elastomer compounds that depend on the compound composition and curing process [Bhowmick, 1994].

Various compounds are used to construct the diverse anatomy of a tire. A tire includes several plies of liners, skids, strips, guards, sidewalls, and tread caps made of assorted compounds. The elastomers used in this study are a blend of KM rubber, which is a mixture of synthetic and natural elastomers for tire tread applications. The material was specially prepared by Michelin and followed a recipe similar to the one in Table 3.2.

*Table 3.2: Generic tire compound example for tread area of the tire [Bhowmick, 1994].*

Common Name	Chemical Name	Parts
SBR	Styrene Butadiene Rubber	75.0
-	Polybutadiene Rubber	25.0
-	Carbon Black	75.0
Aromatic Oil	Highly Aromatic Processing Oil	40.0
Antioxidant	-	1.0
Antiozonant	-	1.5
WAX	Parafinic wax	1.0
HST	Stearic Acid	2.0
ZNO	Zinc Oxide	3.0
Sulfur	Soluble Sulfur	2.0
CBS	Cyclohexylbenzothiazyl Sulfenamide	1.6
PVI	-	0.2

The Poisson's ratio for elastomers is about 0.5, the highest on the scale of Poisson ratios. The high Poisson ratio, and viscoelastic response of elastomers demonstrates the flexibility of the material and presents the challenge in elastomer machining. The viscoelastic response of elastomers is described by Bhowmick [1994] as a combination of

coil springs and dashpots. According to Bhowmick, stretching the compound increases its resistance as more load is applied. One way to offset the flexibility of elastomers is to increase their stiffness with cryogenic cooling. One advantage of elastomer properties is their low thermal conductivity coefficient (0.13 W/mK). Because of the low thermal conductivity coefficient, elastomers can be cooled and remain at reduced temperatures for an extended period of time. At cryogenic temperature elastomers transition into a glassy phase where machining was thought to be possible.

Another way to offset the viscoelastic response and high Poisson ratio of elastomers is to constrain the material in a machining fixture. It is standard practice to secure workpieces in metal working applications from movement. However, in elastomer machining it is also necessary to constrain the material from elastic deflection. Constraining the material enhances the stiffness of the workpiece by preventing elongation and contraction in other coordinate directions while applying a cutting load. The use of an appropriate machining fixture will be discussed in the next section. Cryogenic cooling and the use of workpiece fixturing need to be examined to help identify parameters and conditions that facilitate elastomer machining.

### **3.1 References**

Bhowmick, A. K., Hall, M. M., and Benarey, H. A., 1994, *Rubber Products Manufacturing Technology*, Marcel Dekker, Inc.

Callister, C., 1997, *Materials Science and Engineering*, 4<sup>th</sup> Ed., Wiley.

Gere, J. M., and Timoshenko, S. P., 1997, *Mechanics of Materials*, 4<sup>th</sup> Ed., PWS Publishing Co.

Incropera, F. P., and DeWitt, D. P., 1996, *Fundamentals of Heat and mass Transfer*, 4<sup>th</sup> Ed., Wiley.

## 4 FIXTURE DESIGN

In addition to elastomers apparent need of constraint in fixturing due to its material properties, preliminary tests confirmed the requirement for secure fastening. An elastomer workpiece (295mm x 14.7 mm x 10mm) fastened to the work table with clamps was pulled away from the clamps and lifted from the table when tested with an up milling end mill. Based on preliminary milling tests, good fixture design for the workpiece is essential for elastomer machining experiments. The fixture shown in Figure 4.1 was designed to provide adequate and consistent support for the workpiece. The fixture consists of a base, rail, and a top plate.

The aluminum base and steel top plate are about 229 mm wide ( $Y$  direction) and 197 (mm) long ( $X$  direction). The width of span,  $W$ , on the top plate in Figure 4.1 was 19.1 mm wide making it sufficiently large to accommodate all tools while providing adequate structural support. Note the overhanging elastomer workpiece at the end of the fixture. The fixture length was limited according to the size of the dynamometer it was to be mounted on. The height,  $h$ , on the base shown in Figure 4.2 was set to be 9.1 mm, which is smaller than the 10 mm thickness of the elastomer plate in order to provide the required clamping force.

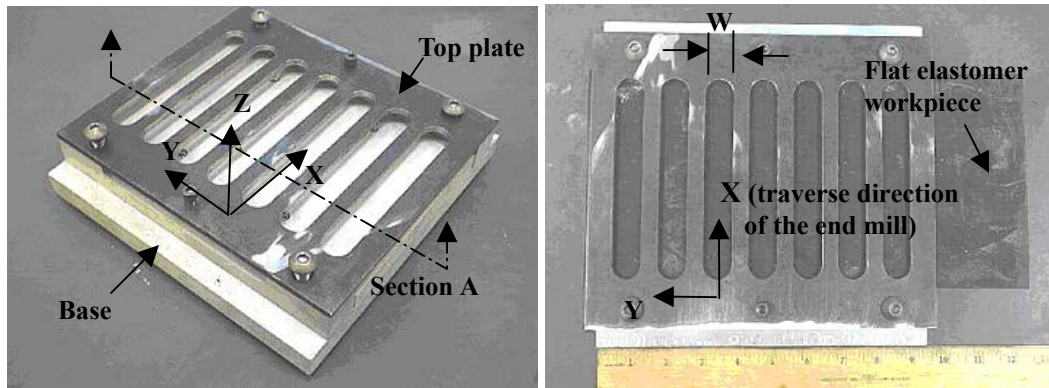


Figure 4.1: Fixture for end milling of elastomer A) base and top plate with slots and B) overhead view with elastomer workpiece.

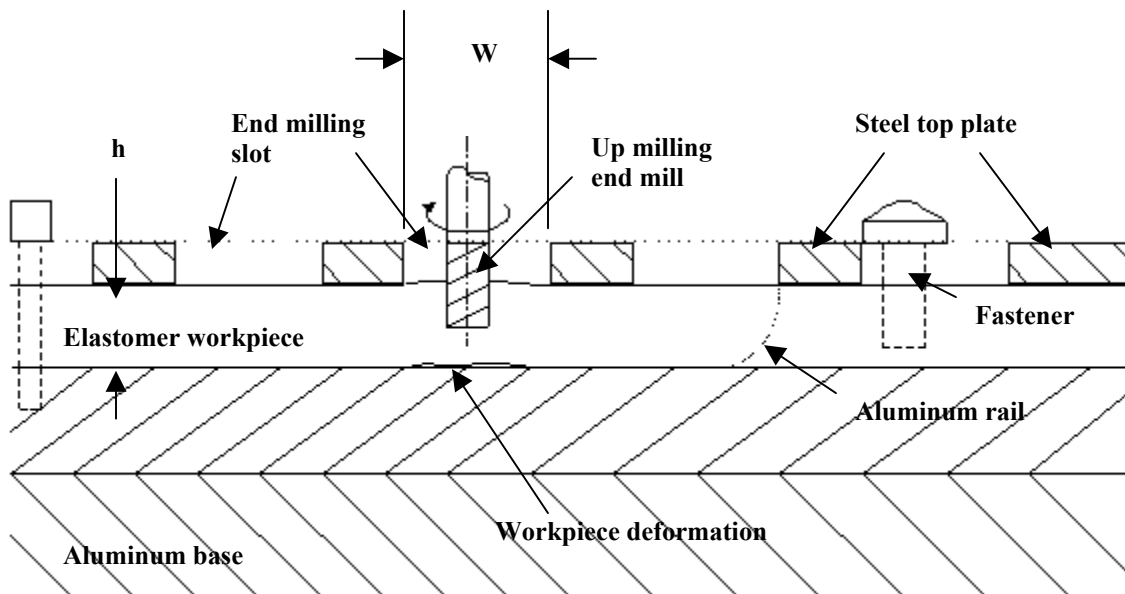


Figure 4.2: Cross section A from Figure 4.1 of fixture for elastomer machining showing end milling slots and workpiece deformation.

The top plate consisted of seven slots allowing an end mill to move across the flat elastomer workpiece with a consistent path for all tests. The steel top plate was 4.75 mm thick. The length of a slot was about 133 mm, which was adequate to reach the steady state cutting condition for the end mill's 114 mm length of travel. The steel top plate, base and side rails act to constrain the material from elastic deflection. Constraining the



material enhances the stiffness of the workpiece by preventing expansion and contraction in other directions while cutting. A study on the stiffness of the elastomer workpiece was performed using ANSYS Finite Element Analysis software, to help determine the effects of the workpiece fixture.

#### **4.1 Finite Element Analysis of Elastomer Workpiece Stiffness**

The finite element method was used to evaluate and compare the stiffness of the elastomer workpiece. The workpiece was constrained by the fixture and machined by end mills of three different diameters. ANSYS finite element analysis software and its mesh generator were used to model the workpiece for cuts made with each of the three diameter end mills. The cut was assumed to be in the middle of the fixture slot and a symmetric boundary condition was applied to the cut. Because of the symmetric boundary condition only half of the workpiece was modeled. The finite element meshes for cutting with 3.18, 6.35, and 12.7 mm diameter end mills are shown in Figure 4.3.

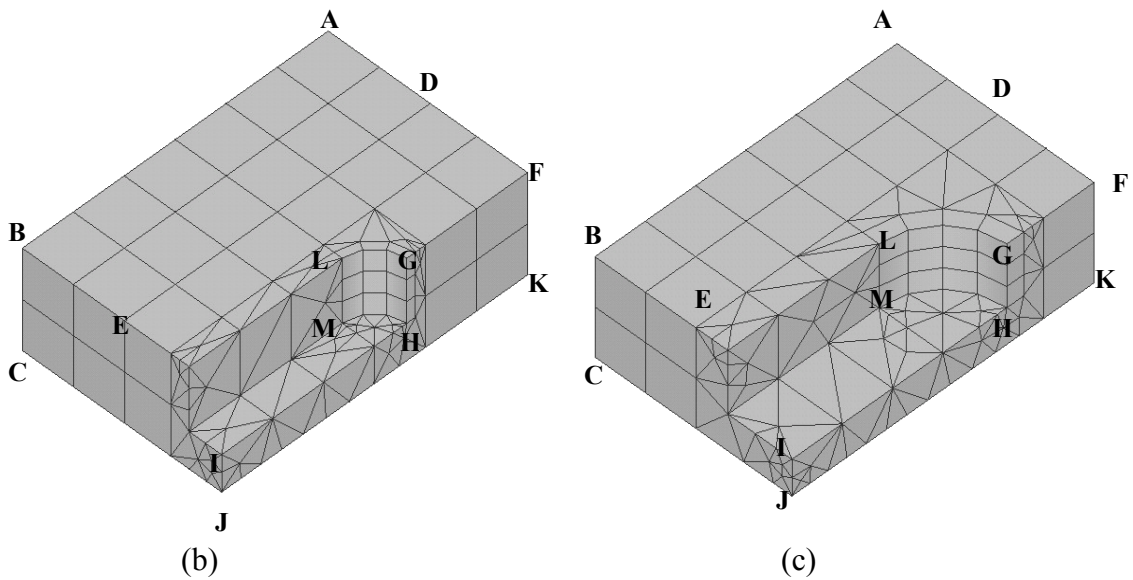
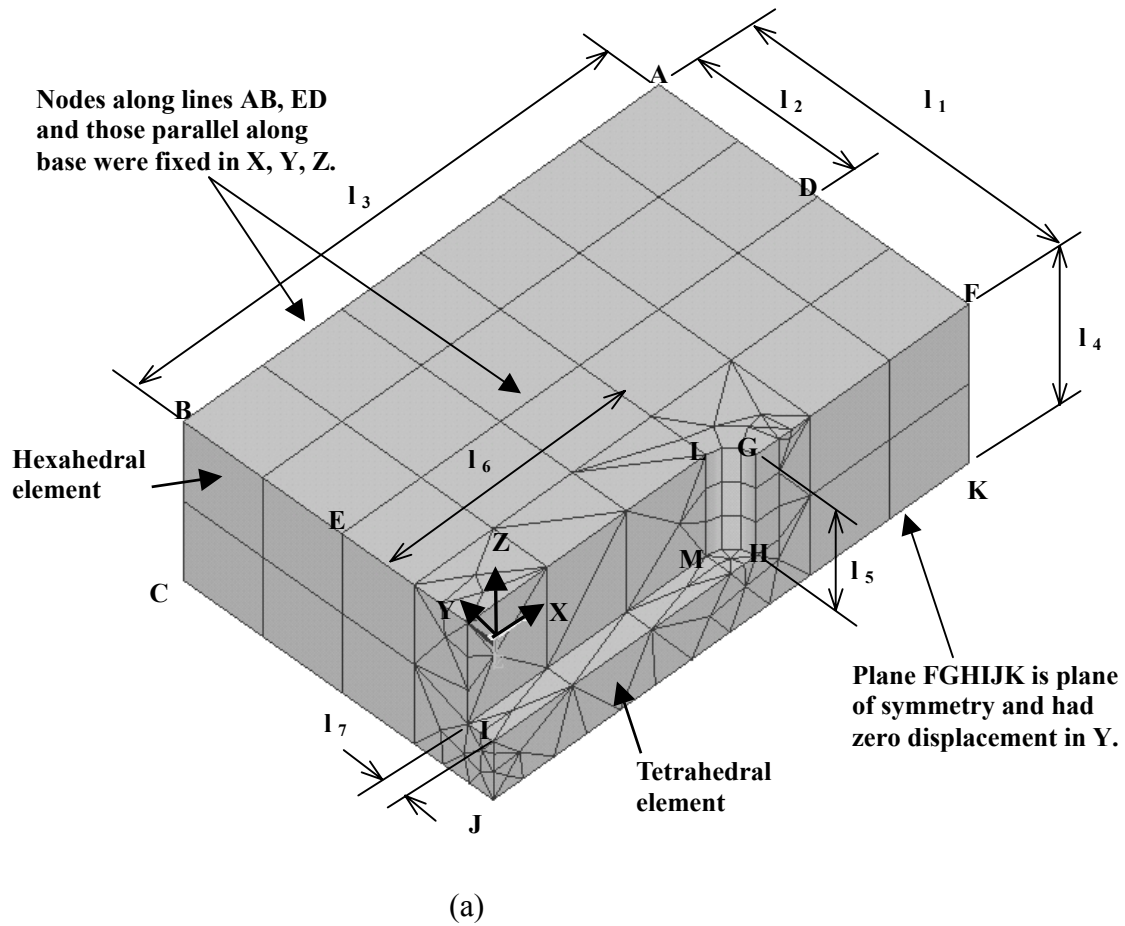


Figure 4.3: Description of three dimensional finite element meshes and boundary conditions for the elastomer workpieces machined by (a) 3.18 mm diameter end mill, (b) 6.35 mm diameter end mill, and (c) 12.70 mm diameter end mill.

Two types of three-dimensional elements were used to model the elastomer. One is the 9-node, 27-degree-of-freedom tetrahedral element and another is the 20-node, 60-degree-of-freedom hexahedral element shown in Figure 4.3 (a). Nodes along lines AB and DE and the line passing through point C and parallel to line AB and DE are fixed in all three ( $X$ ,  $Y$ , and  $Z$ ) directions for all three meshes as indicated in Figure 4.3. Additionally, due to the symmetry boundary condition, all nodes on plane FGHIJK have zero displacement in the  $Y$  direction and are free to move in  $X$  and  $Z$  directions for all three meshes. There are seven key dimensions to the finite element meshes, as illustrated in Figure 4.3(a), and are denoted from  $\mathbf{l}_1$  to  $\mathbf{l}_7$ . The six parameters  $\mathbf{l}_1 - \mathbf{l}_6$  are the same for all meshes and correspond to the following dimensions:

$\mathbf{l}_1 = 19.55$  mm, width of the steel segment of the top plate and the half width of the fixture slot combined.

$\mathbf{l}_2 = 10$  mm, width of the steel segment of the fixture top plate constraining the workpiece.

$\mathbf{l}_3 = 30$  mm, length of workpiece segment modeled.

$\mathbf{l}_4 = 10$  mm, thickness of elastomer workpiece.

$\mathbf{l}_5 = 6.35$  mm, depth of cut used for Finite Element Analysis.

$\mathbf{l}_6 = 15$  mm, length of tool travel on workpiece segment model.

The length  $\mathbf{l}_7$ , which equals half of the tool diameter, is the only parameter that varies for each of the meshes. The dimension of  $\mathbf{l}_7$  equals 1.59, 3.18, and 6.35 mm for the meshes in Figure 4.3(a), (b), and (c), respectively. Note that the depth of cut in the

finite element model,  $l_5$ , was set at 6.35 mm, somewhat larger than the 3.81 mm depth of cut programmed in the end milling experiments. This is used as a conservative estimate to model the increase in the depth of cut observed during milling when up milling forces lift the workpiece.

During end milling, the cutting force is concentrated along the cutting edges of the end mill. The cutting edges move across the quarter cylindrical surface represented by GHML in Figure 4.3. The Finite element model assumes a traction stress is uniformly distributed in the Z direction on the quarter cylindrical surface. Actually, deformation of the workpiece under such a moving load is dynamic and difficult to analyze. Therefore, a parameter called the effective stiffness,  $k_e$ , was defined to compare the stiffness of the workpiece machined by different size end mills. The effective stiffness,  $k_e$ , was defined as:

$$k_e = \frac{2F}{d_{Gz}} \quad (4-1)$$

where  $F$  is the resultant force of the uniform traction stress on the quarter cylindrical surface GHML and  $d_{Gz}$  is the Z direction displacement at point G. Point G is the middle point of the circular arc on the top surface of the workpiece and the point of maximum Z deflection due to the traction stress. The traction stress on the quarter cylindrical surface GHML, is shown in Figure 4.4.

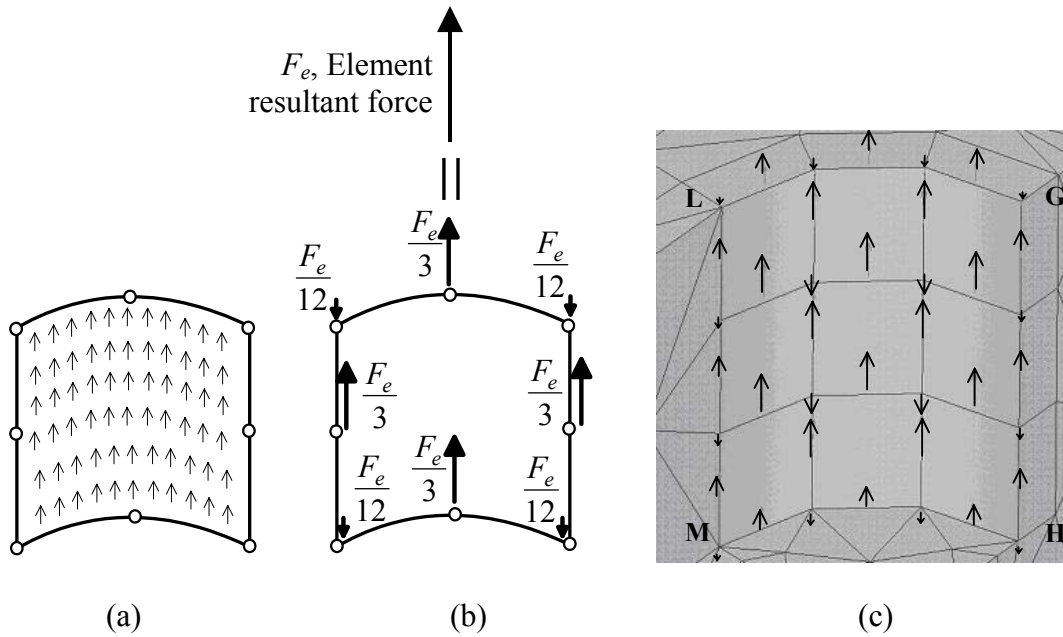


Figure 4.4: Traction stress (a) uniformly distributed on the quarter cylindrical surface in the Z direction, (b) at the eight nodes of a hexahedral element with the element resultant force,  $F_e$ , and (c) distributed as force vectors on the elements of the quarter cylindrical surface.

The force,  $2F$ , in Eq. (4-1) is equal to the total force applied on the quarter cylindrical surface. The traction stress deforms the workpiece, and the displacement at the point of maximum deflection, point G, is measured for the stiffness calculation.

The effective stiffness  $k_e$  was calculated by first converting the traction stress shown in Figure 4.4(a) to the nodal forces on an element with eight nodal points. The procedure for determining the consistent nodal forces described in Cook, et al. [1999] was used for this portion of the analysis. Once the consistent nodal forces were found for the eight node hexahedral element, the forces were applied to the nodes on the elements of the quarter cylindrical surface GHML, as shown in Figure 4.4(c). Finite element analysis simulations were then performed for the three models using an elastic modulus of 2 MPa and Poisson's ratio of 0.49 as shown in Table 3.1.

Three traction stresses were chosen based on reasonable maximum displacement and used for all three models. A comparison of the computed effective stiffness,  $k_e$ , for the three uniformly distributed traction stresses of 0.285, 0.570, and 1.14 N/mm<sup>2</sup> in the three models according to end mill diameters of 3.18, 6.35, and 12.7 mm are summarized in Table 4.1.

*Table 4.1: Results of Finite Element Analysis for the effective stiffness of elastomer workpiece machined using three diameters of end mill.*

Milling tool diameter (mm)	Traction stress (N/mm <sup>2</sup> )	Resultant force on the quarter cylinder, $F$ (N)	Z displacement at point G, $d_{Gz}$ (mm)	Effective stiffness, $k_e$ (N/m)	Average effective stiffness (N/m)
3.18	0.285	4.51	1.17	7,688	7,663
	0.570	9.03	2.39	7,566	
	1.14	18.1	4.67	7,734	
6.35	0.285	9.03	1.80	10,012	9,983
	0.570	18.1	3.63	9,954	
	1.14	36.1	7.23	9,984	
12.7	0.285	18.1	3.14	11,509	11,530
	0.570	36.1	6.27	11,511	
	1.14	72.2	12.5	11,571	

Table 4.1 also lists the resultant force on the quarter cylinder,  $F$ , and the Z direction displacement of point G,  $d_{Gz}$ , which was calculated from the finite element simulation. It was found that the effective stiffness,  $k_e$ , is nearly constant for the three traction stresses for each end mill. The average effective stiffnesses for end milling with a 3.18, 6.35, and 12.7 mm diameter milling tool were 7,663, 9,983, and 11,530 N/mm. The increase in effective stiffness with increasing tool diameter is apparent. The effective stiffness increased by 30% and 15% when the size end mill was increased from 3.18 to 6.35 mm and 6.35 to 12.7 mm diameter, respectively. The change in tool diameter during cutting had a significant influence on the appearance of the machined groove. The influence of

tool size on the appearance of the machined groove may be related to the change in effective stiffness of the workpiece with changing tool diameter and will be discussed in following segments.

For comparison, the three workpiece models for the three size end mills were run for a commonly machined metal. The elastic modulus and Poisson's ratio of steel (200 GPa and 0.3) were simulated with the same models. With a steel workpiece the effective stiffness increased dramatically, about 84,000 times larger than elastomer, when the size end mill increased from 3.18 to 6.35 mm and 6.35 to 12.7 mm diameter. The results of the Finite Element Analysis for steel and elastomer workpieces indicate that the effective stiffness of elastomers is significantly lower than that of steel and that the effective stiffness of elastomers varies with tool size. The Finite Element Analysis results confirm the concept that fixture design is a fundamental subject for elastomer machining.

Another way to increase the rigidity of elastomers is by cryogenic cooling. With the use of cooling and a fixture to constrain the material, several end milling tests were prepared.

## **4.2 References**

Cook, R. D., Malkus, D. S., and Plesha, M. E., 1999, *Concepts and Applications of Finite Element Analysis*, Wiley.

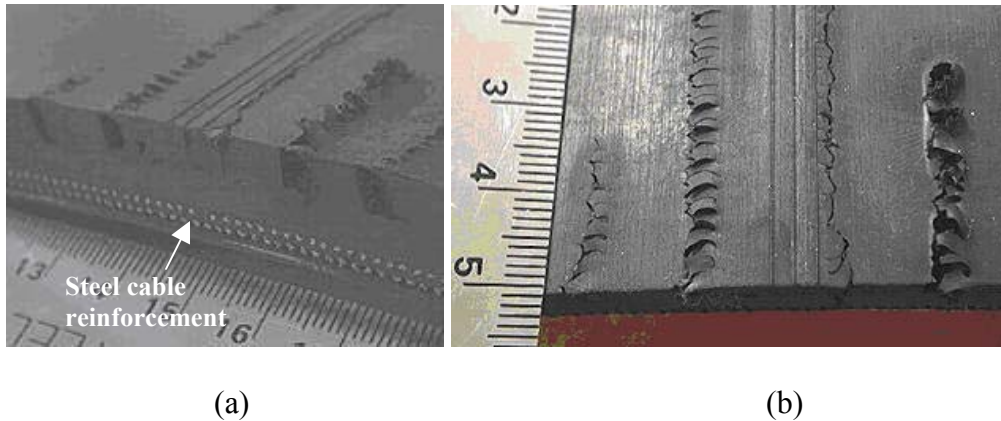
## **5 TEMPERATURE AND MILLING PARAMETERS**

To distinguish mechanisms that can lead to effective rubber machining a depth of cut of 3.81 mm is established for cutting. Cutting depth is held constant so that the effects of other parameters could be observed. The effects of spindle speed and feed rate are the most important parameters to study. The spindle speed and feed rate directly affect the thickness of the chip being removed from the workpiece, which is related to cutting forces. From preliminary tests of trial and error a spindle speed of 4200 rpm and feed rate of 12.7 mm/s were chosen to test the 13 tools.

### **5.1 Preliminary Elastomer Machining Tests**

Due to the very low elastic modulus and large elongation to fracture of elastomers, machining of elastomers is different than machining of metals. To understand the differences in machining elastomers, preliminary milling tests were conducted. For this test, a 4.76 mm diameter high-speed steel up milling end mill was used to cut an elastomer tire segment with the spindle speed of 3600 rpm, feed rate of 0.42 mm/s, and depth of cut of 6.35 mm. Figure 5.1 shows the workpiece with several machined grooves.





*Figure 5.1: Results of preliminary elastomer end milling tests that failed to make a clear cut groove on a workpiece with steel cable reinforcement (a) front view and (b) overhead view.*

As shown in Figure 5.1, the resulting machined surface was rough with burrs along the cut surface of the workpiece. Note the steel cable reinforcement in the elastomer tire segment. The steel cable reinforcement added structural support to the tire segment workpiece and was not used in the regular elastomer samples for the remainder of the experiments. As shown in Figure 5.1, the elastomer workpiece surrounding the machining area can deform significantly due to machining forces. The down milling end mill is used in wood and plastic machining to reduce similar surface damage. Subsequent preliminary tests with down milling configuration tools on room temperature elastomer tire segments generated clear grooves with no burrs on the surface. The absence of the steel belt reinforcement in the regular samples emphasizes the importance of a workpiece fixture for machining elastomers.

## **5.2 Overview of Experiments**

As mentioned earlier, elastomers exhibit a viscoelastic response to applied force, so a fixture was designed to control the workpiece stiffness. Additionally, solid carbon dioxide or dry ice was used to cryogenically cool elastomers to  $-78.6^{\circ}\text{C}$  and offset the

elastic properties of the workpiece. Using the machining fixture and cryogenic cooling a series of 7 experiments was devised and performed. The first three experiments tested all 13 tools at 4200 rpm, and 12.7 mm/s feed rate, and at room temperature, 0°C, and cryogenic or -78.6°C. The last four experiments tested two tools that performed well in the previous three experiments for a series of feed rates and spindle speeds at room temperature and cryogenic temperature. The 0°C temperature condition used in Experiment II was eliminated from testing after it produced similar results to Experiment I, which used the room temperature condition. A summary of the 7 experiments discussed is presented in Table 5.1.

*Table 5.1: Summary of seven end milling experiments on flat elastomer samples.*

Experiment Number	Tools	Workpiece Temperature (°C)	Feed rate (mm/s)	Spindle speed (rpm)
I	1-13	23.0	12.7	4200
II	1-13	0	12.7	4200
III	1-13	-78.6	12.7	4200
IV	6	23.0	2.12, 6.35, 10.6, 14.8	2900, 4200, 5500
V	6	-78.6	2.12, 6.35, 10.6, 14.8	2900, 4200, 5500
VI	8	23.0	2.12, 6.35, 10.6, 14.8	2900, 4200, 5500
VII	8	-78.6	2.12, 6.35, 10.6, 14.8	2900, 4200, 5500

*Table 5.2: Parameter matrix used for testing in Experiments IV – VII.*

Spindle Speed (rpm)	Feed rate (mm/s)			
	2.12	6.35	10.6	14.8
5500	Test 1	Test 2	Test 3	Test 4
4200	Test 5	Test 6	Test 7	Test 8
2900	Test 9	Test 10	Test 11	Test 12

Experiments I – III consisted of 13 tests, one test for each tool at the machining parameters defined in Table 5.1. Experiments IV – VII consisted of 12 tests that followed a parameter matrix sequence. The parameter matrix contained 4 tests for each

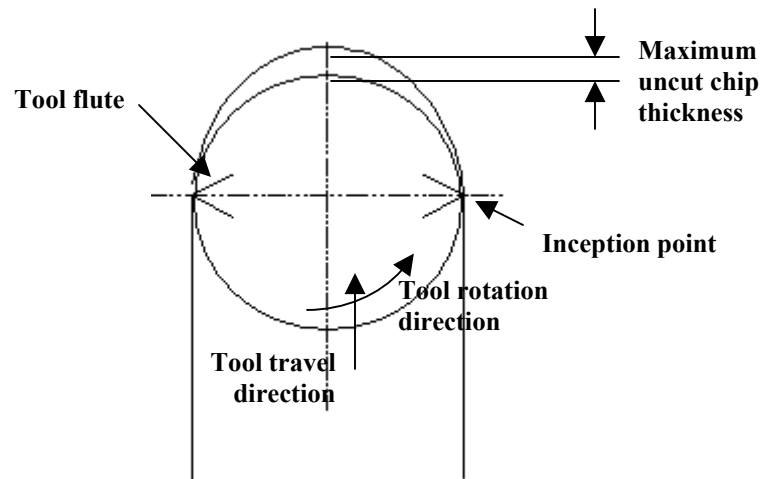
spindle speed corresponding to the 4 feed rates shown in Table 5.1. A description of the parameter matrix used in Experiments IV – VII is shown in Table 5.2.

### 5.3 Overview of Mechanisms that Influence Elastomer Machining

The combination of parameters for Experiments IV – VII was chosen to attempt to identify mechanisms for efficient elastomer machining. Mechanisms of effective elastomer machining were theorized to lie in a relationship between feed rate, spindle speed and the cutting forces. The parameters of feed rate and spindle speed are directly related to the cutting forces through the thickness of the uncut chip removed from the workpiece. The uncut chip thickness can be calculated by kinematics according to the equation:

$$t_{\max} = \frac{FR}{SS} \frac{60}{4} 1 \times 10^{-3} = \text{maximum uncut chip thickness } (\mu m) \quad (5-1)$$

where  $FR$  is the feed rate of the cutting tool in mm/s, and  $SS$  is the spindle speed in rpm. Equation 5-1 is derived from the length of time it takes a tool to rotate from the inception of the cut to the point of maximum uncut chip thickness while traversing the workpiece as represented in Figure 5.2. The remaining terms in Equation 5-1 correspond to the number of flutes on the tool and conversion factors. If the conversion factors are considered as scaling factors and neglected, the extra terms can be simplified to a parameter in the denominator corresponding to the number of flutes. This quantity then becomes the feed rate divided by the product of the spindle speed and the number of flutes, which is referred to as the chip load by Onsrud Cutter's webpage [Onsrud, 2001]. The relationship between the machining parameters and the cutting forces through the maximum uncut chip thickness will be further discussed in subsequent sections.



*Figure 5.2: Description of maximum uncut chip thickness for a two-flute tool.*

In investigating the relationship of the cutting forces and machining parameters, lower cutting forces are beneficial due to less friction between the workpiece and tool, less heat generation, and longer tool life. However, the force quantity is not solely representative of elastomer machining results. Because of elastomer's unusual properties compared to other materials, it was uncertain whether forces could determine the degree of efficiency. The qualitative aspect of elastomer machining was also considered to help determine the effects of machining parameters and conditions on elastomer machining.

## 5.4 References

Onsrud Cutter LP – Online Troubleshooting Guide. Website of Online Information, 2001. <http://www.onsrud.com/ts.php?page=28>

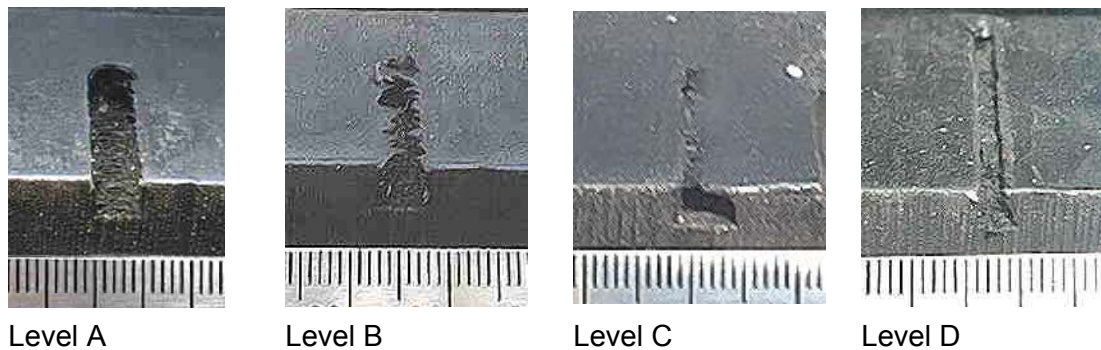
## 6 EXPERIMENTATION

Milling tests were conducted on a HAAS VF1 CNC vertical machining center. All machining tests were conducted without coolant. Seven sets of milling experiments were conducted. The process parameters of these experiments are summarized in Table 5.1. In Experiment I, thirteen end mills were used to machine a groove in an elastomer workpiece at room temperature. Experiments II and III were conducted under identical parameters, but under reduced temperature conditions. Based on favorable milled groove surfaces achieved in Experiment I for Tool 6, twelve additional tests were conducted with this tool for three rotational speeds (2900, 4200, and 5500 rpm) and four feed rates (2.12, 6.35, 10.6, and 14.8 mm/s) in Experiment IV. Experiment V consisted of the same twelve tests with an elastomer temperature of  $-78.6$  °C (solid carbon dioxide cooled). Two final series of tests were conducted with an up milling tool (Tool 8), the up milling equivalent of Tool 6, for room temperature and solid carbon dioxide cooled conditions in Experiments VI and VII. A total of 87 end-milling tests were conducted.

Several criteria were used to evaluate the results of the elastomer machining tests and address the affects of temperature conditions and machining parameters on cutting effectiveness. During milling, the fixture was mounted on a 3-axis Kistler piezoelectric dynamometer to measure components of the end milling forces. For each test, milling forces were measured, chips were collected, and the appearance of the machined groove was recorded.

## 6.1 Appearance of Machined Grooves

As demonstrated in the preliminary end milling tests, the capability of a milling tool to efficiently remove material and generate a neat and burr-free groove is an important performance indicator for tool selection. The surface appearance of the milled cut was observed and categorized into four levels as shown in Figure 6.1 .



*Figure 6.1: Examples of qualitative ratings for machined elastomer grooves.*

Level A, in Figure 6.1 corresponded to a burr-free and clear groove, which is the best surface. Level B was a clear-milled groove, but with some residual burrs on the surface. A thin layer of residual material that covered a clear-milled groove characterized level C. Level D was a blocked groove, which was unacceptable. It is noted that the loose elastomer material inside the groove was removed for all levels except D, where it could not be removed. The above system was employed in each test of the seven experiments to assign qualitative ratings to machined grooves.

## 6.2 Effect of Tool Geometry

Since there was little information available pertaining to proper tool selection for elastomer milling, a large number of thirteen end mills was initially selected for testing. These tools represented a wide range of sizes (3.18, 6.35, and 12.7 mm diameter), tool

materials (high speed steel and carbide), cutting configurations (up and down milling), number of flutes (one and two flute), and cutting tip geometry. Top and side views of these end mills and other basic tool parameters are shown in Figure 2.2. The appearance of the machined grooves for Experiments I – III is summarized in Table 6.1.

*Table 6.1: Qualitative results for grooves machined in Experiments I – III.*

Experiment	Tool												
	1	2	3	4	5	6	7	8	9	10	11	12	13
I	<b>D</b>	<b>D</b>	<b>D</b>	<b>D</b>	<b>B</b>	<b>A</b>	<b>B</b>	<b>C</b>	<b>C</b>	<b>C</b>	<b>C</b>	<b>A</b>	<b>A</b>
II	<b>D</b>	<b>D</b>	<b>D</b>	<b>D</b>	<b>B</b>	<b>A</b>	<b>B</b>	<b>C</b>	<b>C</b>	<b>C</b>	<b>C</b>	<b>A</b>	<b>A</b>
III	<b>D</b>	<b>D</b>	<b>A</b>	<b>B</b>	<b>B</b>	<b>A</b>	<b>B</b>	<b>B</b>	<b>C</b>	<b>C</b>	<b>C</b>	<b>A</b>	<b>A</b>

As mentioned previously, the end mills can be grouped into three series. The appearance of grooves machined with tools from each series was compared to provide insight into elastomer machining based upon basic tool features like number of flutes, cutting configuration, tool material, and size.

### 6.2.1 Tool Size

The six grooves machined by Tools 12 and 13 have the A appearance rating. Note that tools 12 and 13 are the largest of the group (12.7 mm diameter). The six tests performed with tools 12 and 13 indicate that the effective stiffness of the workpiece, which is larger when machined by a larger diameter end mill, is a significant factor in producing a clear groove. In contrast, Tools 2 and 4, also standard series tools but with smaller diameters (3.18 and 6.35 mm in diameter, respectively), did not produce a clear groove. Similarly, Tool 7 (6.35 mm in diameter), which has the same tool geometry as Tool 13 (12.7 mm in diameter) but is a smaller size, only produced a B-rated groove. The effect of tool size to effectively machine a clear groove was further confirmed by the poor results of Tools 1 and 2. These two 3.18 mm diameter tools failed to generate a clear-cut

groove (D-rating) for all three experiments including the solid carbon dioxide cooled elastomer workpiece in Experiment III. The lower stiffness of the workpiece machined by smaller diameter tools is an essential factor that affects elastomer machining performance.

### **6.2.2 Up and Down Milling Configuration**

Tools 6, 12, and 13, all down milling tools, performed very well as indicated by the A rated groove that they produced for all Experiments I, II, and III under both room and reduced temperatures. Tools 5 and 7, which are both 6.35 mm diameter down milling tools, also produced good grooves (B-rating) for all Experiments I, II, and III. The down milling configuration pushes the chip into the workpiece, and helps produce a neat surface.

### **6.2.3 Tool Material and Number of Flutes**

Only the wood rout series and O-flute series tools were made of carbide. Carbide Tools 5, 6, 8, and 10 compared to standard series tools of similar size, geometry and milling configuration suggests carbide tools may have an advantage in cutting elastomers. However, the same comparison made between the smaller size tools (3.18 mm diameter) suggest evidence to the contrary. Therefore, the evidence on the effect of tool material in machining elastomers is inconclusive.

The four pairs of 6.35 mm tools can compare milling configuration. The down milling tools in the pair generated higher appearance ratings on the grooves except for Tool 4. Tool 4 is the only 6.35 mm down milling tool to produce grooves with a D rating. As seen in Figure 6.2, the D level grooves produced by Tool 4 suggest two flutes may be beneficial in elastomer machining.


























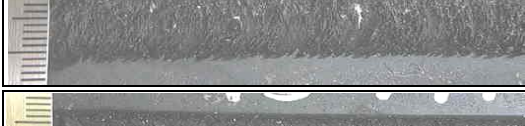


Tool#	Experiment I (Room temp)	Experiment III (Solid carbon dioxide cooled)
1		
2		
3		
4		
5		
6		
7		
8		
9		
10		
11		
12		
13		

Figure 6.2: Grooves machined by the 13 tools in Experiments I and III.

Tools 6 and 8 with the wood rout tip generally performed higher than standard series tools with similar geometry for the 6.35 mm tools. Tool 6 was the only 6.35 mm tool to produce A-ratings of the four pairs, and Tool 8 was the only up milling tool of the group to generate a B-rating at the cryogenic condition. No conclusive evidence can be drawn about the advantages of tools in the O-flute series opposed to standard series because they presented comparable results.

### **6.3 Effect of Workpiece Temperature**

Cooling the elastomer workpiece in solid carbon dioxide improved the effectiveness of tools for removing elastomer work material. For some tools, such as Tools 3, 4, and 8, the improvement was significant. Comparing the results of groove appearance in Experiments I and II, the freezer cooled elastomer (Experiment II) did not show significant improvement.

### **6.4 Effect of Feed Rate and Spindle Speed**

Tools 6 and 8 were selected for a more complete test matrix at four feed rates and three spindle speeds. Both tools have two flutes and are made of carbide. Tool 6 has a down milling and Tool 8 has an up milling configuration. Table 6.2 shows results of groove appearance for Experiments IV (room temperature) and V (solid carbon dioxide cooled) by Tool 6 and Experiments VI (room temperature) and VII (solid carbon dioxide cooled) by Tool 8. As mentioned previously, the maximum uncut chip thickness changes according to changing feed rate and spindle speed. The maximum uncut chip thickness was calculated for the parameters used in Experiments I – VII and presented in Table 6.3.

Table 6.2: Qualitative results of grooves machined in Experiments IV – VII.

Legend: **A:** clear groove.  
**B:** clear groove with residual burrs on the surface.  
**C:** Thin layer of elastomer on surface covering a clear groove.  
**D:** Blocked groove.

Experiment IV (Tool 6, room temp.)					Experiment V (Tool 6, solid carbon dioxide cooled)				
Spindle Speed (rpm)	Feed rate (mm/s)				Spindle Speed (rpm)	Feed rate (mm/s)			
	2.12	6.35	10.6	14.8		2.12	6.35	10.6	14.8
2900	<b>A</b>	<b>A</b>	<b>B</b>	<b>B</b>	2900	<b>A</b>	<b>A</b>	<b>B</b>	<b>B</b>
4200	<b>A</b>	<b>A</b>	<b>A</b>	<b>B</b>	4200	<b>A</b>	<b>A</b>	<b>A</b>	<b>B</b>
5500	<b>A</b>	<b>A</b>	<b>A</b>	<b>A</b>	5500	<b>A</b>	<b>A</b>	<b>A</b>	<b>A</b>

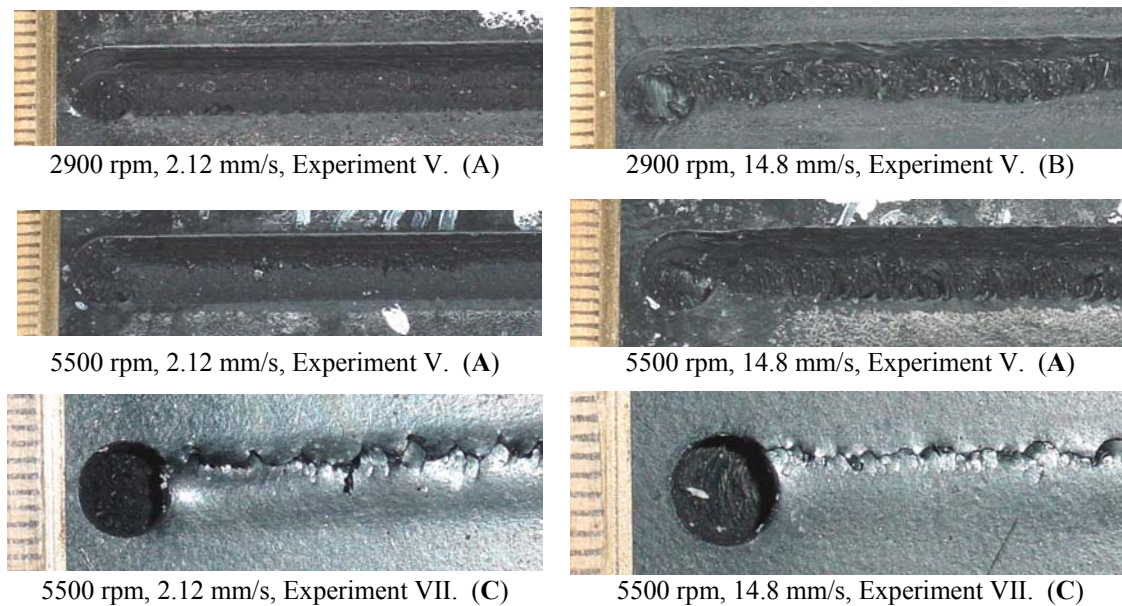
Experiment VI (Tool 8, room temp.)					Experiment VII (Tool 8, solid carbon dioxide cooled)				
Spindle Speed (rpm)	Feed rate (mm/s)				Spindle Speed (rpm)	Feed rate (mm/s)			
	2.12	6.35	10.6	14.8		2.12	6.35	10.6	14.8
2900	<b>C</b>	<b>C</b>	<b>C</b>	<b>C</b>	2900	<b>C</b>	<b>C</b>	<b>C</b>	<b>C</b>
4200	<b>C</b>	<b>C</b>	<b>C</b>	<b>C</b>	4200	<b>C</b>	<b>C</b>	<b>C</b>	<b>B</b>
5500	<b>C</b>	<b>C</b>	<b>C</b>	<b>C</b>	5500	<b>C</b>	<b>C</b>	<b>C</b>	<b>C</b>

Table 6.3: Calculation of uncut chip thickness for parameters in Experiments IV – VII.

Spindle Speed (rpm)	Maximum uncut chip thickness ( $\mu\text{m}$ ) (for two flute end milling tools)				
	Feed rate (mm/s)				
	2.12	6.35	10.6	12.7	14.8
2900	11.0	32.8	54.8	65.7	76.6
4200	7.57	22.7	37.9	45.4	52.9
5500	5.78	17.3	28.9	34.6	40.4

The significant advantage of a down milling tool was obvious, as demonstrated by the good performance of Tool 6 in Experiments IV and V compared to Tool 8 in Experiments VI and VII. Note that A-rated grooves were produced at the highest spindle speed in Experiments IV and V. This observation indicates that high spindle speed is beneficial in elastomer machining and may be due to the smaller uncut chip thicknesses at higher spindle speed. It also indicates that high feed rate may not be advantageous for elastomer machining. Three grooves with B appearance rating were observed at high

feed rates in tests run at 2900 and 4200 rpm in Experiments IV and V. The results of a few tests from Experiment V and VII are displayed in Figure 6.3.



*Figure 6.3: Grooves machined in Experiments V and VII, () indicates groove appearance rating.*

Figure 6.3 shows the machined groove corresponding to the four corners of the test matrix in Experiment V, for spindle speeds of 5500 and 2900 rpm and feed rates of 2.12 and 14.8 mm/s. The deterioration of the groove appearance to level B at 2900 rpm and 14.8 mm/s in Experiment V can be seen. A comparison between the two grooves machined by Tool 8 in Experiment VII, 5500 rpm spindle speed and 2.12 and 14.8 mm/s feed rates and the grooves machined by Tool 6 for the same parameters, are also shown in Figure 6.3. Sharper grooves machined by Tool 6 under the same end milling condition were apparent. Photographs in Figure 6.3 also illustrate the deterioration of groove shape at high feed rate while the spindle speed remains the same. For the same spindle speed, the width of groove decreased proportionally with increasing feed rate. This is possibly due to the large uncut chip thickness generated in elastomer machining at high feed rate.

A further discussion of the effects of changing uncut chip thickness in elastomer machining will follow.

In addition to the appearance of the machined grooves, chip debris from each machining test was collected to help evaluate the results of elastomer machining tests.

## 7 CHIP MORPHOLOGY

The thirteen end mills were used in Experiments I, II, and III to machine an elastomer workpiece at room, freezer-cooled, and solid carbon dioxide cooled temperatures. The elastomer chips generated in Experiments I–VII were collected and examined. End mills of diameters 3.18, 6.35, and 12.7 mm were used in the experiments. Ideally, the half-circle uncut chips were 4.99, 9.97, and 19.9 mm long for milling with 3.18, 6.35, and 12.7 mm diameter tools. However, the actual size of most of the observed chips was much smaller. The small chip sizes observed indicates that chip breakage occurs frequently during end milling of elastomers.

In general, chip formation in machining can be categorized as forming continuous, discontinuous, or serrated chips [Komanduri, 1981]. The serrated chip with accompanying adiabatic shear band is commonly observed in machining materials that exhibit poor thermal properties with either low thermal conductivity or low specific heat. For materials with such poor thermal properties, the heat generated in the shear zone does not have time to escape. The collected heat raises the temperature in the shear zone and leads to thermal softening and adiabatic shear band formation. Titanium is an example material that exhibits such thermal characteristics. The thermal conductivity of titanium alloys is low, about 7 W/m·K, as compared to about 35–40 W/m·K for steels. In machining titanium alloys, adiabatic shear band formation occurs under a wide range of cutting conditions [Trent, 2001, Shaw, 1986, Yang, 1999, Xie, 1996].

Elastomers have even lower thermal conductivity, about 0.15 W/m·K, than titanium and may also promote adiabatic shear band formation in a chip. Furthermore, the low modulus of elasticity and low stiffness of an elastomer can trigger workpiece vibration

during end milling and create wavy serration marks on the chip surface. In the experiments conducted, both adiabatic shear band and wavy types of serrated chips were observed. Besides these two classical types of chip, other types of elastomer chips were observed and a classification method was developed. In this study, a digital camera with close-up lens was used in cooperation with a Hitachi S-4700 SEM, which can achieve a low 25X magnification.

## **7.1 Chip Classification System**

Optical pictures of elastomer chips machined by Tools 1 to 13 in Experiments I and III are shown in Figure 7.1. The distance between two adjacent marks on the scale shown in this figure is 1 mm. The chips are categorized by both size and morphology. First the chips are classified into five size categories: 1) 1–2 mm, 2) 2–3 mm, 3) 3–4 mm, 4) 4–5 mm, and 5) 5+ mm. Note that various sizes of chip can be generated in one end-milling test. For example, the 1–2 and 3–4 mm size chips are generated by Tool 1 in Experiment I, as seen in Figure 7.1. Other end milling tests, such as Tools 8 and 9 in Experiment III, generated large size chips. The two large diameter tools (12 and 13) did not generate very large chips as expected. The primarily smaller size chip debris in the tests suggests that, compared to the large chip generated by Tool 8 in Experiment III, frequent chip breakage must occur during elastomer end milling.

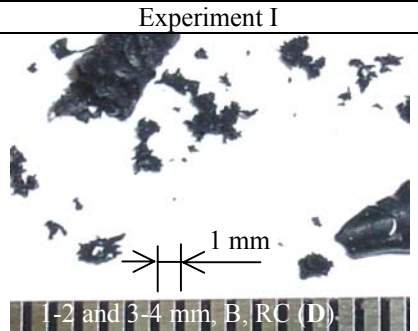

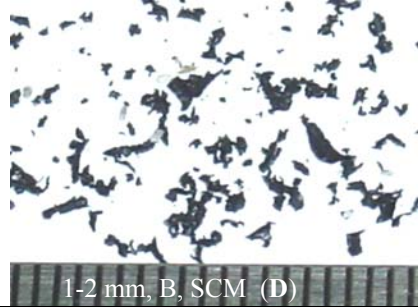

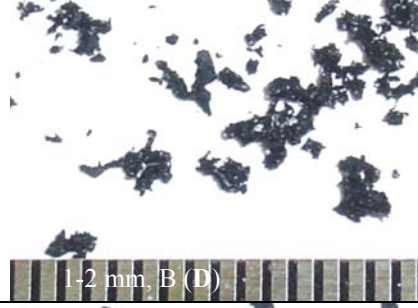
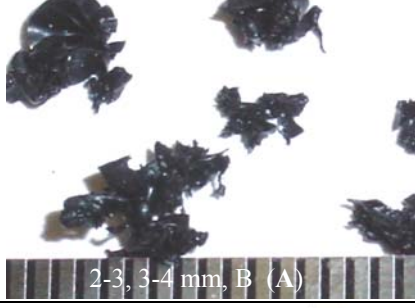


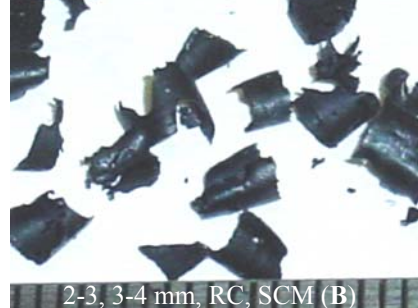
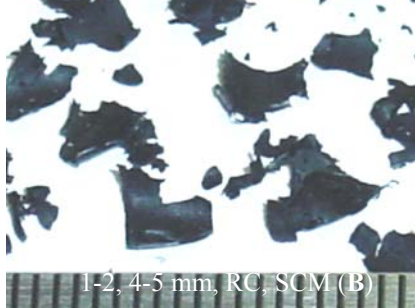
Tool	Experiment I	Experiment III
1		
2		
3		
4		
5		

Figure 7.1: Optical pictures of elastomer chip collected from Experiments I and III, () represents groove appearance rating.



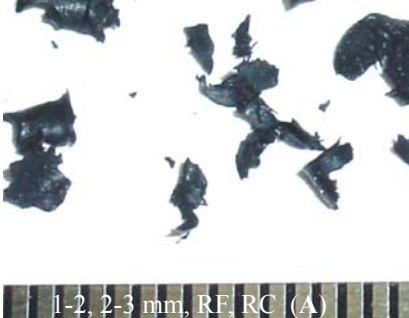
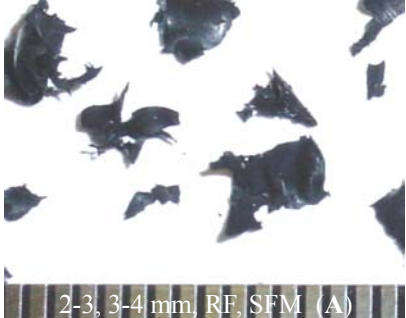
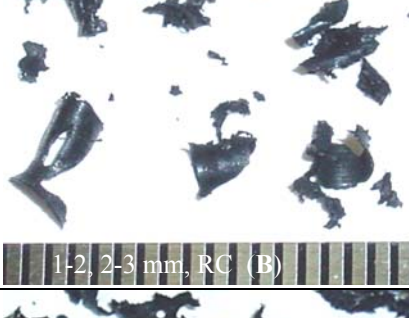
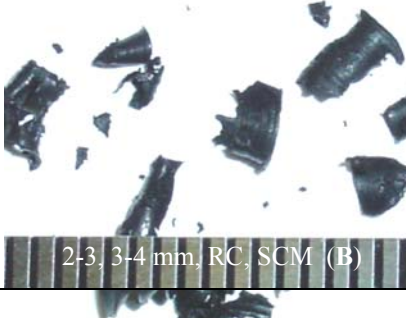


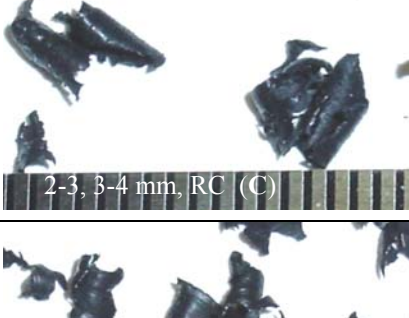
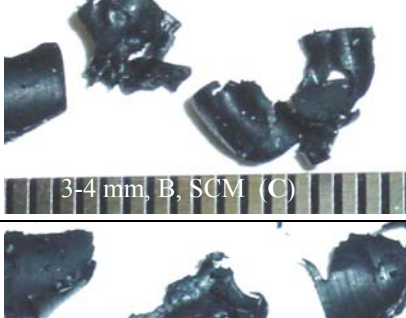


Tool	Experiment I	Experiment III
6		
7		
8		
9		
10		

Figure 7.1: Optical pictures of elastomer chip collected from Experiments I and III, () represents groove appearance rating.

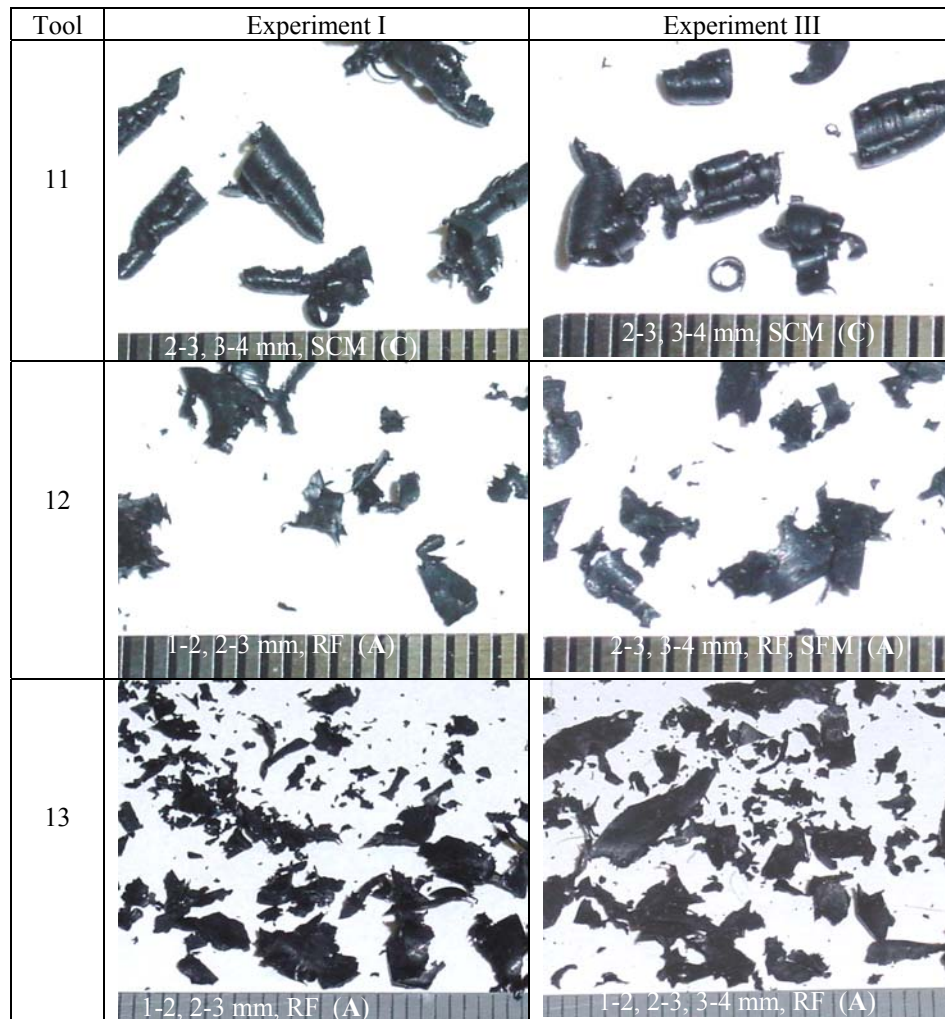


Figure 7.1: Optical pictures of elastomer chip collected from Experiments I and III, () represents groove appearance rating.

The length of an uncut chip cut by the 6.35 mm diameter Tool 8 was 9.97 mm. The 7 mm chip length generated by Tool 8 in Experiment III indicates that, compared to metal cutting, significant elastic recovery occurs during elastomer chip formation processes. The chips from Experiments I and III are presented in Figure 7.1. In general, cooling the elastomer workpiece to cryogenic conditions (Experiment III) created slightly larger chip sizes as shown.

Different chip shapes were observed, as shown in Figure 7.1. Some chips are curled, and others are flat. Some chips have serration marks on the surface, and others have a smooth surface. Some chips are small and cannot be examined clearly using an optical camera with close-up lens. The combination of optical pictures and SEM micrographs were used to classify the chip morphology using the following four-step procedure:

Step 1. Examine if the chip has been burned or melted.

Step 2. Observe if the chip has rough or straight edges in the cutting direction.

Step 3. Inspect if the chip is curled.

Step 4. Look for the serration marks on chip surface.

Based on these four steps, the chips can be categorized into seven different types: B, RC, RF, SCE, SCM, SFE, and SFM as demonstrated in Figure 7.2.

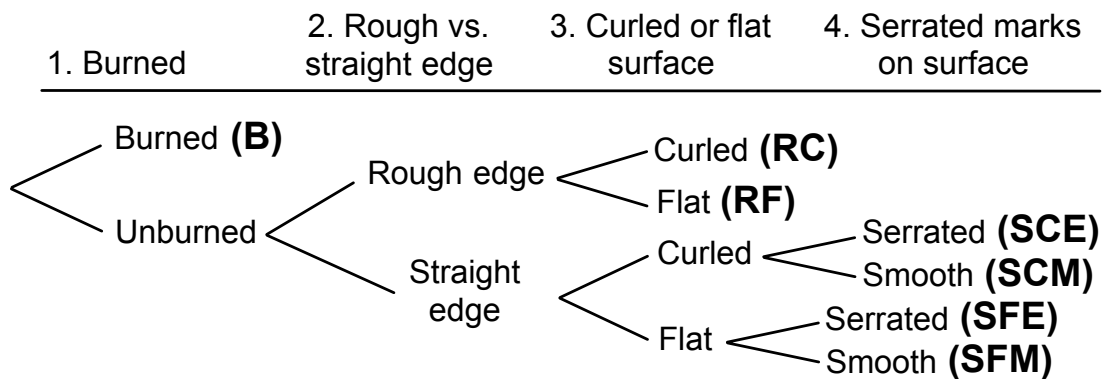


Figure 7.2. The four-step procedure used to categorize chip morphology for an end milled elastomer.

The seven types of chip generated in Experiments I and III are indicated in pictures in Figure 7.1. It is possible that two or three types of chip can be generated for the same

cutting condition. For example, both B and RC chip types were observed as generated by Tool 1 in Experiment I.

## **7.2 Discussion of Chip Types**

A more detailed view of the seven types of chip morphology can be obtained with a SEM. SEM micrographs and discussions of the seven types of chips are summarized in the following.

### **7.2.1 Straight Flat Serrated Chip (SFE)**

An adiabatic shear band shown in Figure 7.3 was observed for Experiment VII at 4200 rpm and 14.8 mm/s feed rate using Tool 8 for end milling a solid carbon dioxide cooled elastomer. A detailed view of the chip surface and the adiabatic shear bands are shown in Figure 7.3(b). The spacing between two adjacent shear bands is about 0.4 mm. The shear band shown in Figure 7.3(b) is very narrow, about 10  $\mu\text{m}$  wide. Among all 87 tests conducted, this is the only one that exhibited adiabatic shear band formation. The end milling conditions for inception of such adiabatic shear bands is not clear. The test was on the edge of the experiment matrix in Table 6.2 with four feed rates and three spindle speeds. End milling with the same feed rate but higher (5500 rpm) and lower (2900 rpm) spindle speeds did not generate chips with similar adiabatic shear bands.

### **7.2.2 Straight Curled Serrated Chip (SCE)**

A curled and serrated chip with wavy serration marks on the surface was observed for some chips as machined by Tool 8 in Experiment III. The optical picture in Figure 7.1 also reveals serration marks on the surface. SEM micrographs in Figure 7.4(a) show the wavy form on a curled SCE chip. These wavy marks were most likely created by vibration of the elastomer workpiece during machining. Although elastomers are

known for their good vibration damping capability, the force created during end milling can still cause the workpiece to vibrate and generate the wavy marks observed on the chip surface. Both the flat SFE and curled SCE chips were observed in this test (Tool 8, Experiment III). Figure 7.4(b) shows the SEM micrograph of a flat SFE chip with wavy marks on the surface.

### **7.2.3 Rough Flat Chip (RF)**

Figure 7.5 shows a sample RF chip with a rough edge and flat surface as generated by Tool 6 in Experiment I (room temperature). Edges along the cutting direction are not straight in the RF type chip.

### **7.2.4 Straight Curled Smooth and Rough Curled Chip (SCM and RC)**

There are two other types of curled chips in addition to the SCE chip shown in Figure 7.4(a). Figures 7.6(a) and 7.6(b) show the SCM chips machined by Tool 11 in Experiments I and III. Both chips have smooth surfaces and straight edges in the cutting direction. The RC type of curled chip, as shown in Figure 7.7(a), was machined by Tool 4 with 2.12 mm/s feed rate and 5500 rpm. This was not one of the standard tests in Experiments I–VII. This chip has rough edges on all sides. Some of type B burned chips can also be seen in Figure 7.7(a).

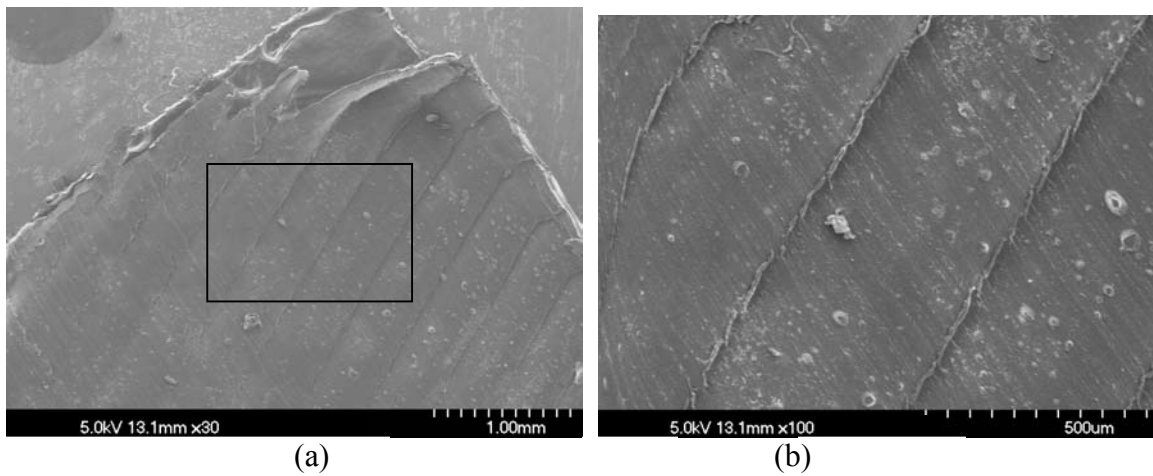
### **7.2.4 Burned Chip (B)**

Smoke could be observed during some of these end milling tests. This indicates that heat generated during end milling was sufficiently high to burn and melt the elastomer material. At high temperature and atmospheric pressure, an elastomer sublimates to a gaseous phase. The gasification of an elastomer could leave a burned surface or edge on the residual chip that did not get totally burned. Figures 7.7(a) and 7.7(b) show SEM

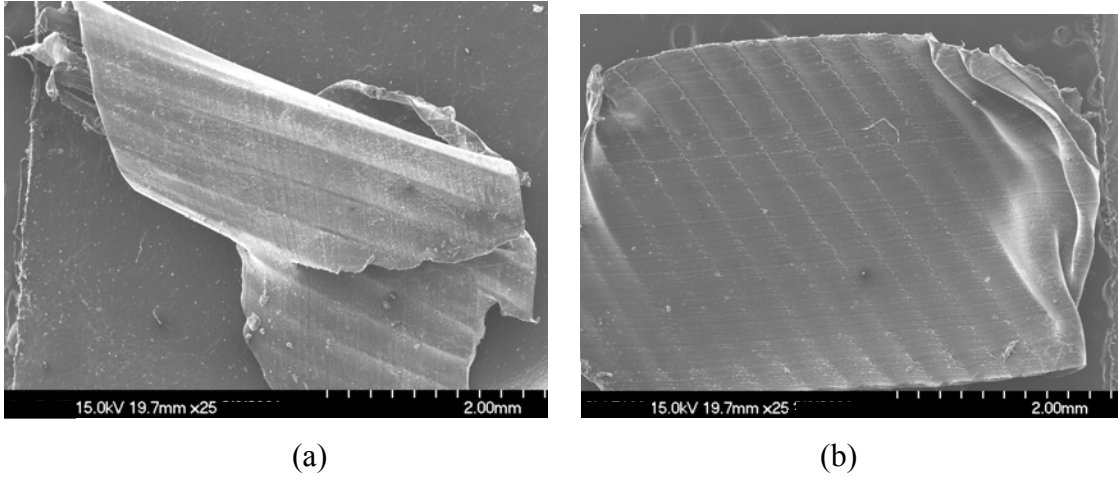
micrographs of a burned chip. As shown in Figure 7.7(a), a burned chip can be small, less than 100  $\mu\text{m}$ , and lumped together. As shown in Figure 7.7(b), edge burning on a chip was also observed.

### 7.2.5 Straight Flat Smooth Chip (SFM)

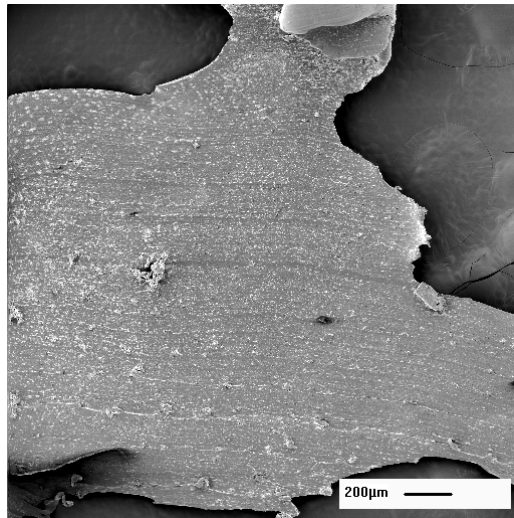
As shown in Figure 7.8, the SFM type of chip which has a straight edge in the cutting direction and a flat and smooth surface was observed for Tool 6 in Experiment V with a 10.6 mm/s feed rate and 4200 rpm spindle speed.



*Figure 7.3: SEM micrographs of adiabatic shear band in the SFE type chip machined by Tool 8 in Experiment VII, 14.8 mm/s feed rate and 4200 rpm spindle speed, (a) overview of the chip and (b) close-up view shear band in the box in (a).*



*Figure 7.4: SEM micrographs of (a) a curled, serrated SCE type chip with wavy marks machined by Tool 8 in Experiment III, (b) a SFE type of chip with the wavy serration mark on the surface.*



*Figure 7.5: SEM micrographs of a RF type of chip machined by Tool 8 in Experiment I.*

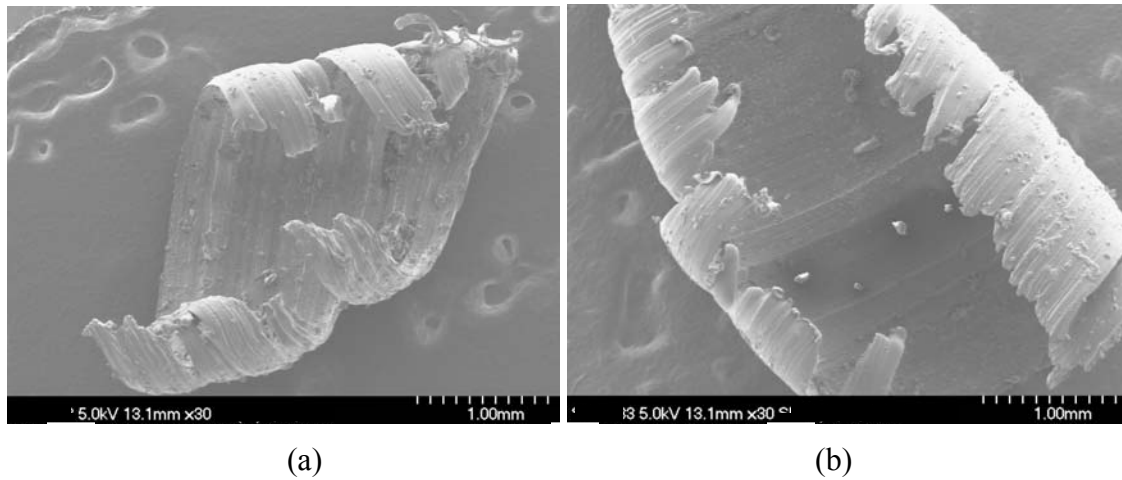


Figure 7.6: SEM micrographs of SCM type curled chip machined by Tool 11 in (a) Experiment I and (b) Experiment III.

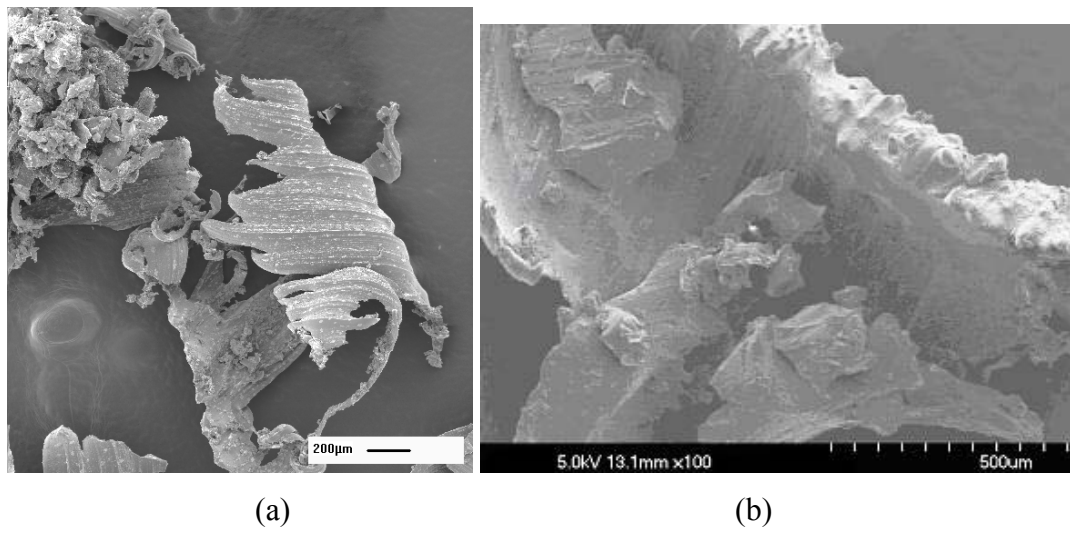
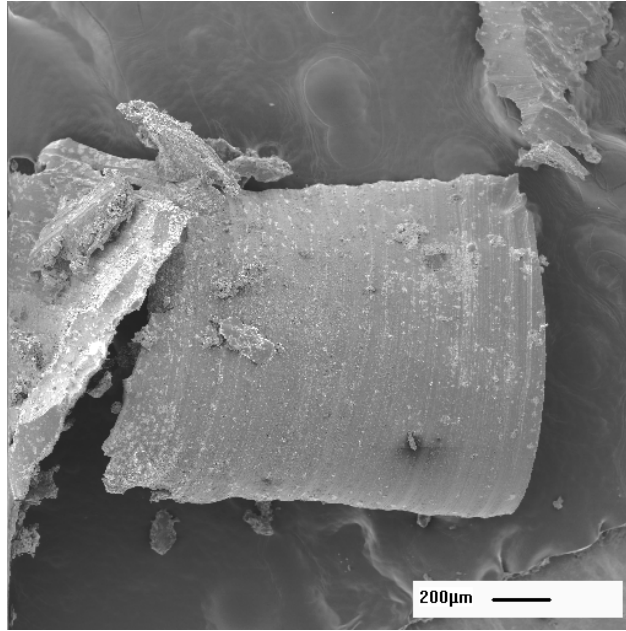


Figure 7.7: (a) The RC and B types of chips machined by Tool 4 with 2.12 mm/s feed rate and 5500 rpm and (b) chip with burned edge, machined by Tool 2 in Experiment I.





*Figure 7.8: SFM chip machined by Tool 4 at 5500 rpm and 14.8 mm/s feed rate.*

### **7.3 Correlation between Chip Characteristics and Groove Appearance**

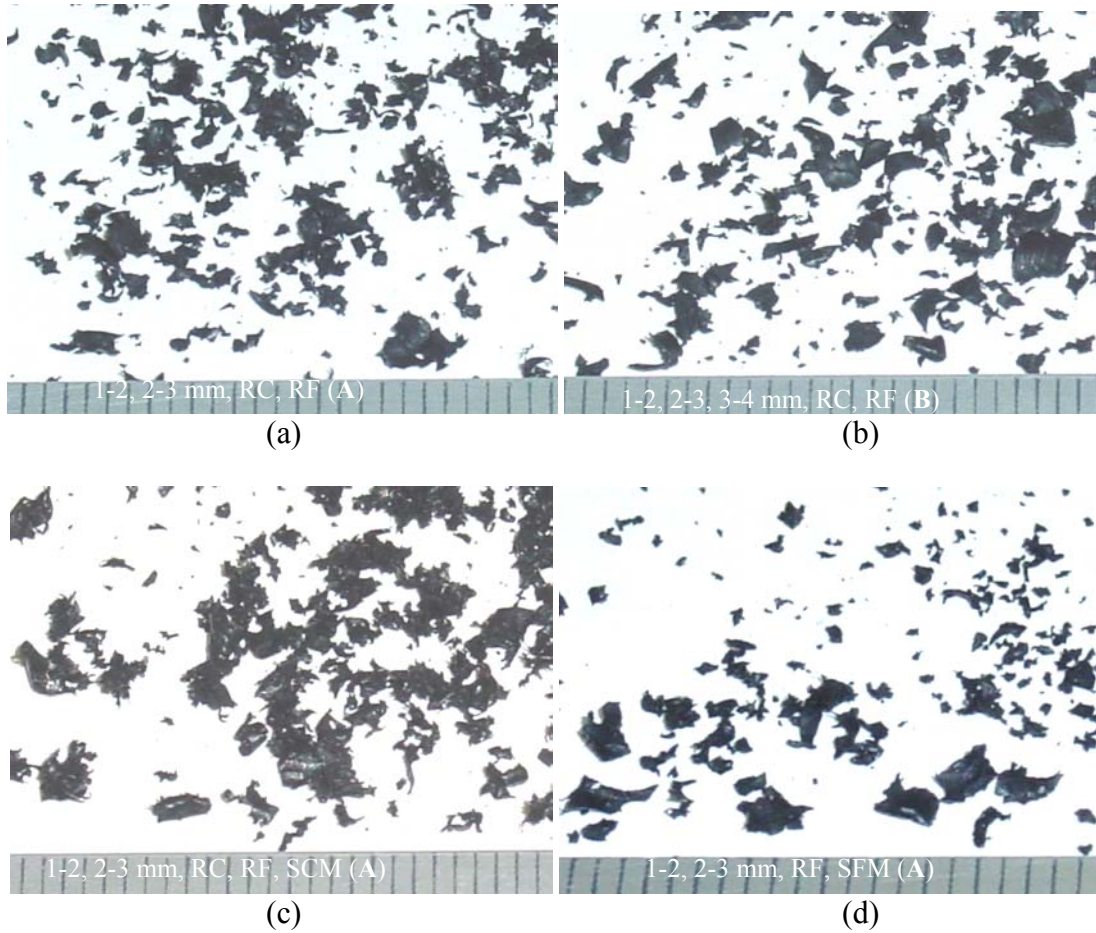
The two large 12.7 mm diameter tools (Tools 12 and 13) did not generate larger size chips as expected. Even when the workpiece was more fully constrained and clear (level A) grooves were formed, the chips produced by Tools 12 and 13 were small, in the 2 to 4 mm range. The cutting Tools that generated large size chips, such as Tools 8 and 10 in Experiment III, exhibited the partially clear B and C level appearance ratings. Both observations signify that the size of the chip does not correlate well with the appearance of the groove and the complexity of the chip formation process.

However, a correlation may exist between the chip morphology and groove appearance. Note that a burned chip is almost always associated with grooves with a blocked or a level D rating groove. Therefore, poor cutting action occurred in the D level grooves with chip burning. The most common type of chip observed were curled chips

and were usually associated with a B or C appearance level groove. Additionally, grooves that showed a clear-cut groove with A level appearance rating were often observed to produce flatter chips.

#### **7.4 Effect of Spindle Speed and Feed Rate on Chip Morphology**

The effect of spindle and feed rates on chip morphology is illustrated in Figure 7.9. Chips corresponding to the four corners of the test matrix in Experiment V (2900 and 5500 rpm and 2.12 and 14.8 mm/s feed) were examined. These four end milling conditions have the same length of uncut chip (9.97 mm) and, as shown in Table 6.3, different maximum uncut chip thickness. End milling at 2900 rpm and 14.8 mm/s feed rate generates a larger chip. This is also the end milling condition that has the largest maximum uncut chip thickness of 76  $\mu\text{m}$ . Many small size chip (1–2 mm) were mixed in all four end milling conditions. This further demonstrates the frequency of chip breakage and the random chip size in end milling elastomers.



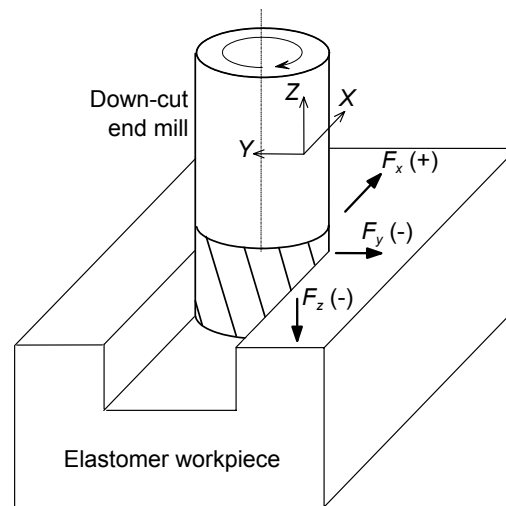
*Figure 7.9: Optical pictures of chip formation in the four corners of the test matrix in Experiment V, Tool 6 at (a) 2900 rpm, 2.12 mm/s feed, (b) 2900 rpm, 14.8 mm/s feed, (c) 5500 rpm, 2.12 mm/s feed, and (d) 5500 rpm, 14.8 mm/s feed. ( ) Represents groove appearance rating of end milled groove.*

## 7.5 References

- Komanduri, R., and Brown, R. H., 1981, "On the Mechanics of Chip Segmentation in Machining," *Journal of Engineering for Industry*, Vol. 103, pp. 33-51.
- Komanduri, R., and von Turkovich, B. F., 1981, "New Observations on the Mechanism of Chip Formation when Machining Titanium Alloys," *Wear*, Vol. 69, pp. 179-188.
- Shaw, M. C., 1986, *Metal Cutting Principles*, Oxford.
- Trent, E. M., and Wright, P. K., 2001, *Metal Cutting*, 4<sup>th</sup> Ed., Butterworth-Heinemann.
- Xie, J. Q., Bayoumi, A. E., and Zbib, H.M., 1996, "A Study on Shear Banding in Chip Formation of Orthogonal Machining," *International Journal of Machine Tool and Manufacture*, Vol. 36, No. 7, pp. 835-847.
- Yang, X., and Liu, C. R., 1999, "Machining Titanium and its Alloys," *Machining Science and Technology*, Vol. 3, No. 1, pp. 107-139.

## 8 FORCES IN END MILLING ELASTOMERS

A Kistler Model 9257B piezoelectric force dynamometer was used to measure three components of force in the 87 elastomer end milling tests. In this section, the end milling force components generated by Tool 6 in Experiments I, III, and V are presented and compared. As shown in Figure 8.1, the  $X$ -axis is defined to coincide with the feed direction and the  $Z$ -axis is along the rotating axis of the end mill tool. The  $Z$ -axis is perpendicular and pointing outward from the surface of the flat elastomer plate. This sign convention was adopted from References [Kline, 1982, Sutherland, 1986, Smith, 1991].  $F_x$ ,  $F_y$ , and  $F_z$  are three force components acting on the workpiece from the rotating end mill. Figure 8.1 shows that due to the feed direction of end mill the  $F_x$  component should be positive in general, and  $F_y$  should be mostly negative. Since the tool pushes the workpiece in the negative  $Z$  direction,  $F_z$  should also remain negative. Note that vibration of the workpiece and end mill could temporarily reverse the force direction, as will be seen later for measured force results.



*Figure 8.1: Definition of the directions of force components and general direction of the three force components generated by down milling Tool 6 on the elastomer workpiece.*

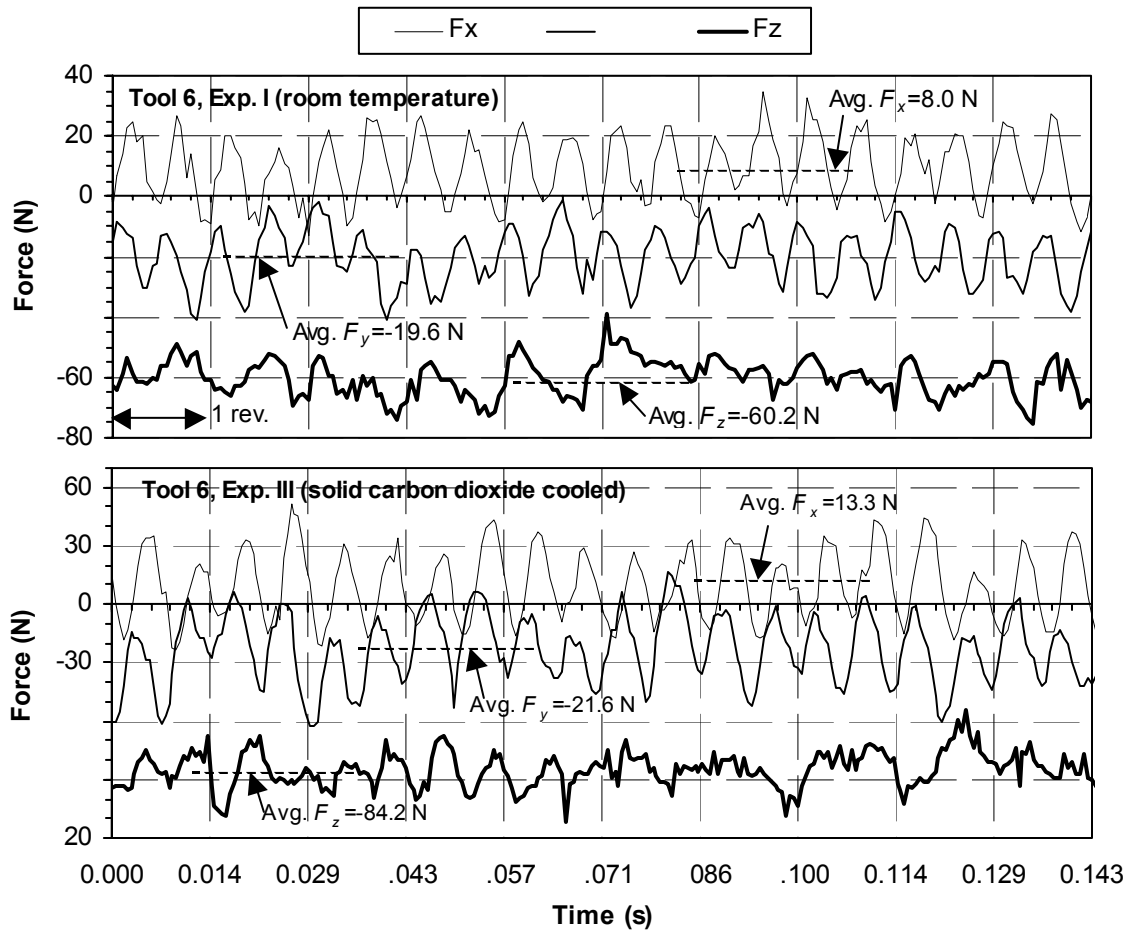


Figure 8.2: Three end milling force components vs. time for Tool 6 in Experiments I and III (4200 rpm and 12.7 mm/s feed rate).

Figure 8.2 shows the measured three  $F_x$ ,  $F_y$ , and  $F_z$  force components for end milling using Tool 6 in Experiments I and III. The force data include 10 revolutions of the end milling tool in the middle of its 114 mm travel across the slot of the fixture. The tool was rotating at 4200 rpm. Each revolution of the two-flute tool took 0.0143 s (70 Hz), as indicated in the time scale marker in Figure 8.2. Some noticeably different force responses were observed for the same tool and parameters cutting the elastomer at room and cryogenic temperatures. Ideally using the two-flute Tool 6, two peaks should occur in the force vs. time traces for each revolution or every 0.0143 s. Such a trend was

obvious for  $F_x$  and  $F_y$  force traces in Experiments I and III. However, it was not clear for  $F_z$ , which sometimes showed only one flat peak during a tool rotation. It is noted that the natural frequency of the dynamometer and fixture is much higher than the 70 Hz tool rotational speed.

Figure 8.2 also shows values of average  $F_x$ ,  $F_y$ , and  $F_z$  components for the two cutting conditions. The data collected during the 114 mm cutting path was used to calculate the average force components. These average force values matched very well with the 0.143 s snap shot of force data in Figure 8.2. For experiments I and III, the average  $F_x$  is 8.0 and 13.3 N,  $F_y$  is  $-19.6$  and  $-21.6$  N, and  $F_z$  is  $-60.2$  and  $-84.2$  N. As expected,  $F_x$  remains positive and  $F_y$  and  $F_z$  remain negative most of the time. Under cryogenic condition, the elastomer workpiece is harder and requires higher machining forces. The magnitude of peak  $F_x$  and  $F_y$  is about 30 N in Experiment III compared with 20 N in Experiment I. The difference in magnitude of  $F_z$  for Experiments I and III is more significant. Since Tool 6 is a down milling tool and the chip is forced downward into the surface, the compliance of the elastomer workpiece at room temperature allows the chip to exit the cutting area and generates a smaller  $F_z$ .

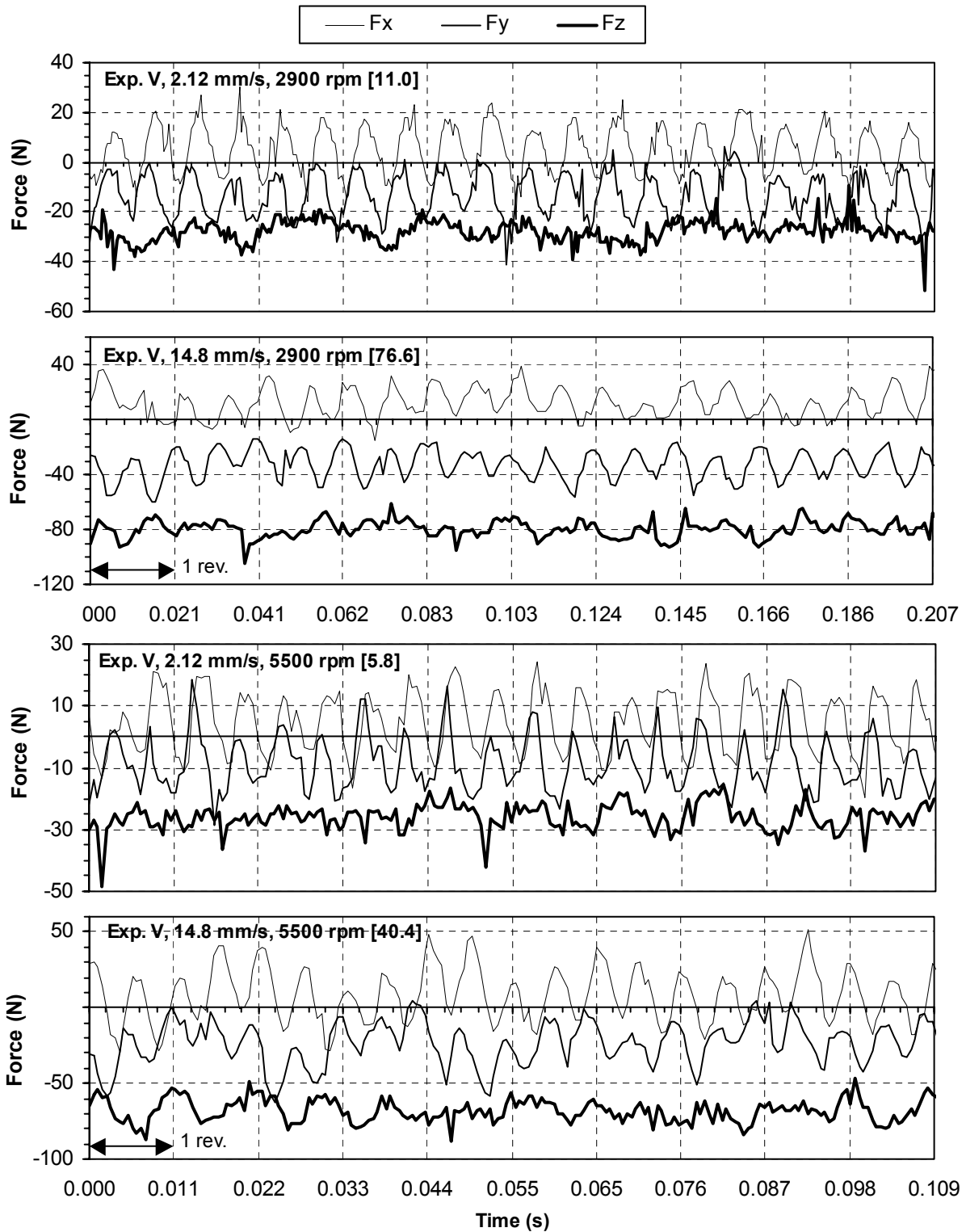


Figure 8.3: Three end milling force components vs. time at the four corners of the test matrix in Experiment V: Tool 6, carbon dioxide cooled workpiece. [ ]: maximum uncut chip thickness in  $\mu\text{m}$ .



To further investigate the effects of tool speed and feed on forces, three force components versus time graphs of selected cutting conditions at the four corners of the test matrix (2.12 and 14.8 mm/s feed rate and 2900 and 5500 rpm) were performed in Experiment V for Tool 6 end milling of solid carbon dioxide cooled elastomer, as shown in Figure 8.3. The data was collected for 10 consecutive tool rotations in the middle of the tool's 114 mm travel along the slot of the fixture. A negative  $F_z$  of about  $-30$  N for 2.12 mm/s feed rate and  $-40$  N for 14.8 mm/s feed rate was observed. Similar to the trend observed in Figure 8.2,  $F_z$  stays in a relatively constant level and does not vary drastically with the tool rotation. Two peaks of  $F_x$  and  $F_y$  in each tool rotation could be seen for all four cutting parameters. Significant variation of the magnitude of peak forces can be observed for both  $F_x$  and  $F_y$  in Figure 8.2. Chip breakage during machining, as illustrated in the previous section, is the likely cause of the fluctuation.

The effect of chip thickness and strain rate could be identified in Figure 8.3. The maximum uncut chip thickness for these four cutting conditions is included in Figure 8.3. The two cutting tests with 2.12 mm/s feed rate have smaller chip thickness and exhibit lower forces. Also, note from Table 6.2 these parameters generated level A groove appearance ratings. The strain-rate hardening effect can be identified by comparing the magnitude of peak forces in two tests at 14.8 mm/s feed rate in Figure 8.3. These two tests have different maximum uncut chip thickness, 76.6 and 40.4  $\mu\text{m}$  for 2900 and 5500 rpm tool speed, respectively. Although milling at 5500 rpm has smaller chip thickness, the level of peak forces for  $F_x$ ,  $F_y$ , and  $F_z$  is about the same: 30 N for  $F_x$ ,  $-40$  N for  $F_y$ , and  $-80$  N for  $F_z$ . Under the same spindle speed the increase in milling forces at higher

feed rate is likely due to the strain-rate hardening of the elastomer material during cutting.

Effects of chip thickness and strain rate in Experiment V are further analyzed in the eight milling tests at 2900 and 5500 rpm from experiment V. Results of the averaged peak forces for  $F_x$ ,  $F_y$ , and  $F_z$  under these eight milling parameters vs. the maximum uncut chip thickness are shown in Figure 8.4.

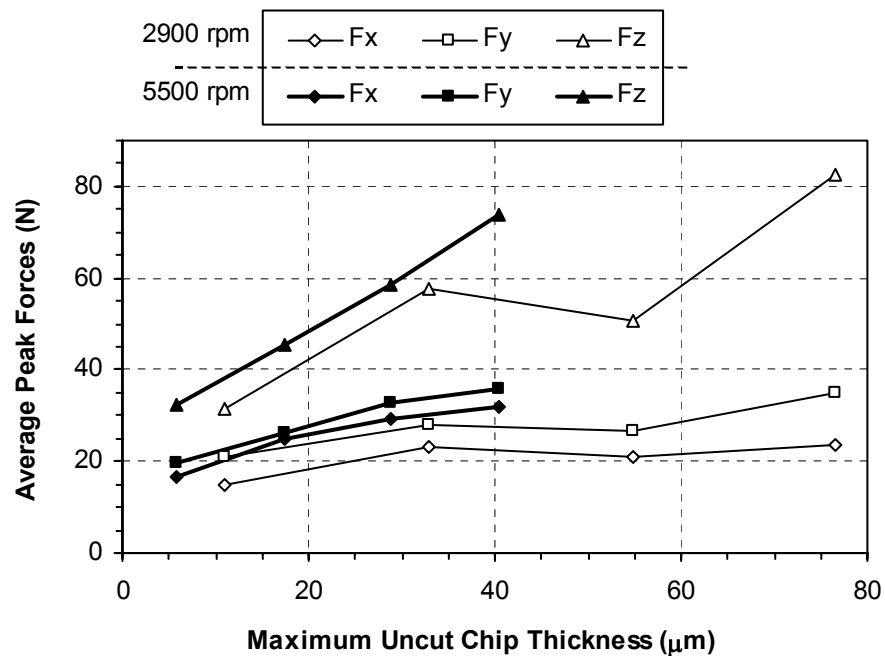


Figure 8.4: Average peak milling forces vs. maximum uncut chip thickness in Experiment V at 2900 and 4200 rpm.

In Figure 8.4, a linear trend of increasing tool forces vs. maximum uncut chip thickness is identified, particularly for milling at 5500 rpm. The four points on the curves corresponds to the peak forces at the four feed rates of each spindle speed. The average peak forces were calculated by averaging the absolute value of 20 consecutive peaks in 10 tool rotations for  $F_x$  and  $F_y$  (two peaks per tool rotation). For  $F_z$ , the peak force was random in nature and 20 peak values were selected and averaged within the time span of

10 tool rotations. The relationship between cutting forces and uncut chip thickness has indicated the potential to use the mechanistic or finite element method to model the elastomer end milling process.

## **8.1 References**

- Kline, W. A., DeVor, R. E., and Lindberg, J. R., 1982, "The Prediction Cutting Forces in End Milling with Application to Cornering Cut," *International Journal of Machine Tool Design and Manufacture*, Vol. 22, pp. 7-22.
- Sutherland, J. W., and DeVor, R. E., 1986, "An Improved Method for Cutting Force and Surface Error Prediction in Flexible End Milling Systems," *Journal of Engineering for Industry*, Vol. 108, pp. 269-279.
- Smith, S., and Tlusty, J., 1991, "An Overview of Modeling and Simulation of the Milling Process," *Journal of Engineering for Industry*, Vol. 113, pp. 169-175.

## 9 CONCLUSION

In this study the end milling of elastomers was investigated by the use of 13 sharp woodworking tools. New innovative methods to cut elastomers could provide cost and time savings to industries producing elastomer products by the use of rubber molds. Additionally, custom markets of low volume production in the tire industry could benefit from an elastomer machining process.

Elastomers high percentage elongation to fracture and visco-elastic properties present a challenge to the subject of elastomer machining. Two ways to offset the effects of elastomers' flexible properties were explored in this project, workpiece fixturing and cryogenic cooling.

It is standard practice to secure work pieces in metal cutting from movement, however, it is also necessary to constrain the material from elastic deflection in elastomer machining. A machining fixture was designed and used to constrain the elastomer material while cutting, and the effects of the support to the workpiece were analyzed using ANSYS finite element analysis software. A parameter,  $k_e$ , called effective stiffness, was defined and used to describe the stiffness of the workpiece machined by different size end mills. The effective stiffness of the elastomer workpiece was found to increase by 30% and 15% when the size end mill used was increased from 3.18 to 6.35 mm and 6.35 to 12.7 mm diameter, respectively.

The flexibility of the workpiece was also reduced with the use of cryogenic cooling. Despite the challenge of elastomers' flexible properties, the material's low thermal conductivity coefficient (0.15 W/mK) is conducive to cooling able to remain at reduced temperature for longer periods of time than most materials.

The cooling of elastomers was only partially investigated. The thermal properties and thermal response of elastomers at cryogenic temperatures has potential in elastomer machining. Other cooling methods could be investigated such as cooling of the machining fixture by internal flushing with chilled water or other coolant. Fixture cooling is commonly used in metal fabrication.

Cooling the elastomer workpiece in solid carbon dioxide to  $-78.6^{\circ}\text{C}$  improved the effectiveness of tools for removing elastomer work material. Other factors that influenced machining results were tool size, the milling configuration of the end mill, and the milling parameters used for testing. Tool geometry varies widely in industry and could be more precisely explored to identify key geometric features to effective elastomer machining.

Of the different size tools, the high performance in groove appearance of the 12.7 mm diameter tools, and the low performance of the smaller diameter, 3.18 mm tools, suggest that the effective stiffness of the workpiece, which is larger when machined by a larger diameter end mills, is a significant factor that effects elastomer machining performance.

The down milling configuration of the cutting tool showed an obvious benefit in generating a clear groove in elastomer machining as demonstrated by the high performance of Tools 6, 12 and 13 at both room temperature and cryogenic conditions. The performance of down milling Tool 6 in experiments IV and V compared with up milling Tool 8 in experiment VI and VII further emphasize the advantage of down milling configuration as apposed to traditional up milling end mills.

Different chip shapes and sizes were observed for the elastomer experiments conducted. A system for classifying chip morphology was developed for 7 types of chip and 5 chip sizes. The appearance of serrated chips with adiabatic shear band was observed for one of the 87 milling tests. Cutting conditions used to generate chip with serration marks in elastomer milling may be a potential research subject. The chips produced by the 13 tools were commonly smaller than the length of the uncut half circle chip length designating the high frequency of chip breakage during elastomer machining. The 2 – 4 mm size chips produced by the 12.7 mm diameter tools indicated rapid chip breakage during milling.

Grooves with level B and C rating frequently contained curled chips and grooves with a level A rating generated more flat chips. Also, type B (burned) chips were observed for tests with a level D rating groove. The observations of the chip debris suggests a correlation between chip morphology and groove appearance. Additionally, in the tests of the four corners of Experiment V larger chips were observed for test at 2900 rpm and 14.8 mm/s than the others and also had a larger uncut chip thickness than the others.

The results of Experiments IV – VII presented evidence that indicates higher spindle speeds in elastomer machining may be beneficial. The higher spindle speed tests in experiments IV and V generated A rating grooves for all feed rates. A mechanism of effective elastomer machining, however, could lie in the relationship between feed rate, spindle speed and cutting forces through size of the uncut chip thickness generated by the combination of parameters. In general, groove appearance was observed to be high for high spindle speeds and low feed rates in and deteriorate in shape and appearance with

increasing feed rate. Accordingly, averaged peak forces were shown to increase with increasing uncut chip thickness. The direct correlation between cutting force, groove appearance, and uncut chip thickness suggests that the uncut chip thickness is an essential mechanism in the effectiveness of elastomer machining.

The linearity of the relationship between cutting forces and maximum uncut chip thickness suggest potential for further exploration of the machinability of elastomers. Modeling applications using the mechanistic or finite element method may be employed by the relationship. Further elastomer machining experimentation may also be modeled upon the basis of minimizing the maximum uncut chip thickness for different combinations of tools and parameters to develop a cutting range for the material.